10

FFLO and Vortex States in Superconductors With Strong Paramagnetic Effect

M. Ichioka, K.M. Suzuki, Y. Tsutsumi and K. Machida
Department of Physics, Okayama University
Japan

1. Introduction

In type-II superconductors (Fetter & Hohenberg, 1969), magnetic fields penetrate into superconductors as quantized flux lines with flux quanta $\phi_0 = hc/2e$, where h is Planck constant, c velocity of light, e electron's charge. Around a flux line, pair potential $\Delta(\mathbf{r})$ of Cooper pair has a vortex structure, where $\Delta(\mathbf{r})$ has phase winding 2π reflecting screening super-current around a flux line. At the vortex core, amplitude $|\Delta(\mathbf{r})|$ is suppressed, and low energy excitations appear within the superconducting gap of the electronic states.

Vortex physics makes important roles in the study of unconventional superconductors, because unconventional characters hidden in the uniform superconducting state at a zero field appear around vortices. For example, in superconductors with anisotropic superconducting gap on Fermi surface in momentum space, electronic states around a vortex show real-space anisotropy in the local density of states (LDOS) $N(E, \mathbf{r})$ around vortex core. The vortex core image is observed by scanning tunneling microscopy (STM) (Hess et al., 1990; Nishimori et al., 2004). Around vortex cores, local zero-energy electronic states at Fermi level are seen as star shape with tails extending toward node or weak-gap directions (Hayashi et al., 1996; 1997; Ichioka et al., 1996; Schopohl & Maki, 1995). From the spatial average of the zero-energy states, we can estimate the zero-energy density of states (DOS) $N(E = 0)$, which determines low temperature (T) behaviors of physical quantities. Due to the differences of electronic states around the vortex core, $N(E = 0)$ shows different magnetic field (H) dependences. These H-dependences are studied to identify the pairing symmetry in the experiments for vortex states, such as, electronic specific heat (Moler et al., 1994; Nohara et al., 1999), electronic thermal conductivity, and paramagnetic susceptibility (Zheng et al., 2002). For example, the H-dependence of low temperature specific heat $C(H)$ is often used to distinguish the presence of nodes in the pairing potential. As for Sommerfeld coefficient $\gamma(H) \equiv \lim_{T\to 0} C(H)/T$, $\gamma(H) \propto H$ in s-wave pairing with full gap, and $\gamma(H) \propto \sqrt{H}$ by the Volovik effect in d-wave pairing with line nodes (Ichioka et al., 1999a;b; Miranović et al., 2003; Nakai et al., 2004; Volovik, 1993). The curves of $\gamma(H)$ are expected to smoothly recover to the normal state value towards the upper critical field H_{c2}. However, in some heavy fermion superconductors, $C(H)$ deviates from these curves. In $CeCoIn_5$, $C(H)$ shows convex curves, i.e., $C(H) \propto H^{\alpha}$ ($\alpha > 1$) at higher fields(Ikeda et al., 2001). This behavior is not understood only by effects of the pairing symmetry. A similar $C(H)$ behavior is observed also in UBe_{13} (Ramirez et al., 1999). The experimental data of magnetization curve $M_{\text{total}}(H)$ in $CeCoIn_5$ show a convex curve at higher fields, instead of a conventional concave curve (Tayama et al., 2002). As an

unconventional behavior of $CeCoIn_5$, the small angle neutron scattering (SANS) experiment reported anomalous H-dependence of flux line lattice (FLL) form factor determined from the Bragg intensity (Bianchi et al., 2008; DeBeer-Schmitt et al., 2006; White et al., 2010). While the form factor shows exponential decay as a function of H in many superconductors, it increases until near H_{c2} for $H \parallel c$ in $CeCoIn_5$. In some heavy fermion superconductors, the paramagnetic effects due to Zeeman shift are important to understand the properties of the vortex states, because the superconductivity survives until under high magnetic fields due to the effective mass enhancement. A heavy fermion compound $CeCoIn_5$ is a prime candidate of a superconductor with strong Pauli-paramagnetic effect (Matsuda & Shimahara, 2007). There at higher fields H_{c2} changes to the first order phase transition (Bianchi et al., 2002; Izawa et al., 2001; Tayama et al., 2002) and new phase, considered as Fulde-Ferrell-Larkin-Ovchinnikov (FFLO) state, appears (Bianchi, Movshovich, Capan, Pagliuso & Sarrao, 2003; Radovan et al., 2003). As for properties of $CeCoIn_5$, the contribution of antiferromagnetic fluctuation and quantum critical point (QCP) is also proposed in addition to the strong paramagnetic effect (Bianchi, Movshovich, Vekhter, Pagliuso & Sarrao, 2003; Paglione et al., 2003). Therefore, it is expected to study whether properties of vortex states in $CeCoIn_5$ are theoretically explained only by the paramagnetic effect. Theoretical studies of the H-dependences also help us to estimate strength of the paramagnetic effect, in addition to pairing symmetry, from experimental data of the H-dependences in various superconductors.

In this chapter, we concentrate to discuss the paramagnetic effect in the vortex states, to see how the paramagnetic effect changes structures and properties of vortex states. The BCS Hamiltonian in magnetic field is given by

$$\begin{aligned}\mathcal{H} - \mu_0 \mathcal{N} = &\sum_{\sigma=\uparrow,\downarrow} \int \mathrm{d}^3\mathbf{r}\, \psi_\sigma^\dagger(\mathbf{r}) K_\sigma(\mathbf{r}) \psi_\sigma(\mathbf{r}) \\ &- \int \mathrm{d}^3\mathbf{r}_1 \int \mathrm{d}^3\mathbf{r}_2 \left\{ \Delta(\mathbf{r}_1, \mathbf{r}_2) \psi_\uparrow^\dagger(\mathbf{r}_1) \psi_\downarrow^\dagger(\mathbf{r}_2) \ + \Delta^*(\mathbf{r}_1, \mathbf{r}_2) \psi_\downarrow(\mathbf{r}_2) \psi_\uparrow(\mathbf{r}_1) \right\}\end{aligned} \tag{1}$$

for superconductors of spin-singlet pairing, with

$$K_\sigma(\mathbf{r}) = \frac{\hbar^2}{2m} \left(\frac{\nabla}{\mathrm{i}} + \frac{\pi}{\phi_0} \mathbf{A} \right)^2 + \sigma \mu_\mathrm{B} B(\mathbf{r}) - \mu_0, \tag{2}$$

$\sigma = \pm 1$ for up/down spin electrons. Suppression of superconductivity by magnetic field occurs by two contributions. One is diamagnetic pair-breaking from vector potential $\mathbf{A}$ in Hamiltonian inducing screening current of vortex structure. And the other is paramagnetic pair-breaking from Zeeman term, which induces splitting of up-spin and down-spin Fermi surfaces as schematically presented in Fig. 1. Due to the Zeeman shift, in normal states, numbers of occupied electron states are imbalance between up-spin and down-spin electrons. The imbalance induces paramagnetic moment. In superconducting state with spin-singlet pairing, formations of Cooper pair between up-spin and down-spin electrons reduce the imbalance, and suppress the paramagnetic moment. However, the paramagnetic moment may appear at place where superconductivity is locally suppressed, such as around vortex core. Therefore, it is important to quantitatively estimate the spatial structure of paramagnetic moment and the contributions to properties of superconductors in vortex states.

One of other paramagnetic effect is paramagnetic pair breaking. When the Zeeman effect is negligible, as in Fig. 1(a), for Cooper pair of up-spin and down-spin electrons at Fermi level, total momentum Q of the pair is zero, i.e., $Q = k + (-k) = 0$. However, in the presence of

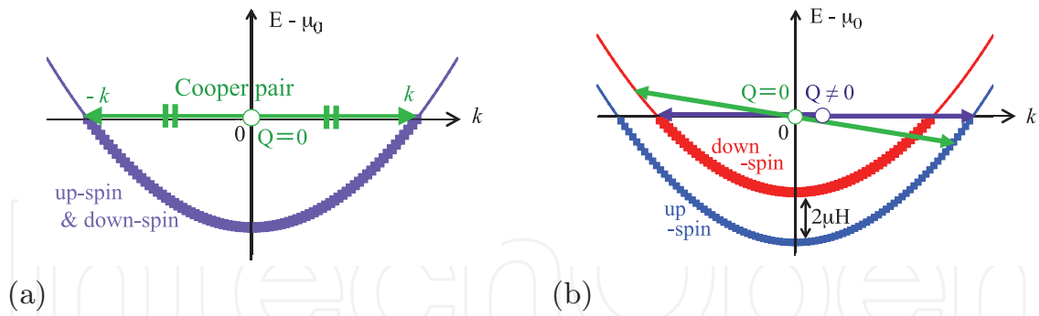

(a) (b)

Fig. 1. Paramagnetic effect by Zeeman shift of energy dispersion is schematically presented. Bold lines indicate occupied states. (a) The case when Zeeman shift is negligible. For Cooper pairs at Fermi level, total momentum $Q = k + (-k) = 0$. (b) When Zeeman shift is significant, the energy dispersions of up-spin and down-spin electrons are separated. When $Q = 0$, the electrons of Cooper pair are not at Fermi level. In FFLO states, $Q \neq 0$ so that electrons of Cooper pair are located at Fermi level.

Zeeman splitting, in order to keep $Q = 0$, Cooper pair is formed between electrons far from Fermi level, as shown in Fig. 1(b). Since the energy gain by this pairing is smaller than that of negligible paramagnetic case, the Zeeman splitting induces paramagnetic pair-breaking of superconductivity. In addition to H_{c2} suppressed by the paramagnetic pair-breaking, it is important to quantitatively estimate the contribution of paramagnetic pair-breaking on properties of vortex states at $H < H_{c2}$.

When paramagnetic effect by Zeeman shift is further significant, transition to FFLO state occurs at high magnetic fields near H_{c2}. In FFLO state, as shown in Fig. 1(b), electrons at Fermi level form Cooper pair with non-zero total momentum ($Q \neq 0$), which indicates periodic modulation of pair potential (Fulde & Ferrell, 1964; Larkin & Ovchinnikov, 1965; Machida & Nakanishi, 1984). When FFLO state appears in vortex state, we have to estimate properties of the FFLO state, considering both of vortex and FFLO modulation (Adachi & Ikeda, 2003; Houzet & Buzdin, 2001; Ichioka et al., 2007; Ikeda & Adachi, 2004; Mizushima et al., 2005a;b; Tachiki et al., 1996). Another system for significant paramagnetic effect is superfluidity of neutral ^{6}Li atom gases under the population imbalance of two species for pairing (Machida et al., 2006; Partridge et al., 2006; Takahashi et al., 2006; Zwierlein et al., 2006). There, we can study vortex state by rotating fermion superfluids, under control of paramagnetic effect by loaded population imbalance.

For theoretical studies of vortex states including electronic structure, we have to use formulation of microscopic theory, such as Bogoliubov-de Gennes (BdG) theory (Mizushima et al., 2005a;b; Takahashi et al., 2006) or quasi-classical Eilenberger theory (Eilenberger, 1968; Klein, 1987). In this chapter, based on the selfconsistent Eilenberger theory (Ichioka et al., 1999a;b; 1997; Miranović et al., 2003), we discuss interesting phenomena of vortex states in superconductors with strong paramagnetic effect, i.e., (i) anomalous magnetic field dependence of physical quantities, and (ii) FFLO vortex states. We study the spatial structure of the vortex states with and without FFLO modulation, in the presence of the paramagnetic effect due to Zeeman-shift (Hiragi et al., 2010; Ichioka et al., 2007; Ichioka & Machida, 2007; Watanabe et al., 2005). Since we calculate the vortex structure in vortex lattice states, self-consistently with local electronic states, we can quantitatively estimate the field dependence of some physical quantities. We will clarify the paramagnetic effect on the vortex core structure, calculating the pair potential, paramagnetic moment, internal magnetic field,

and local electronic states. We also study the paramagnetic effect by quantitatively estimating the H-dependence of low temperature specific heat, Knight shift, magnetization and FLL form factors. For quantitative estimate, it is important to appropriately determine vortex core structure by selfconsistent calculation in vortex lattice states. These theoretical studies of the magnetic field dependences help us to evaluate the strength of the paramagnetic effect from the experimental data of the H-dependences in various superconductors.

After giving our formulation of selfconsistent Eilenberger theory in Sec. 2, we study the paramagnetic effect in vortex states without FFLO modulation in Sec. 3, where we discuss the H-dependence of paramagnetic susceptibility, low temperature specific heat, magnetization curve, FLL form factor, and their comparison with experimental data in $CeCoIn_5$. We also show the paramagnetic contributions on the vortex core structure, and the local electronic state in the presence of Zeeman shift. Section 4 is for the study of FFLO vortex state, in order to theoretically estimate properties of the FFLO vortex states, and to show how the properties appear in experimental data. We study the spatial structure of pair potential, paramagnetic moment, internal field, and local electronic state, including estimate of magnetic field range for stable FFLO vortex state. As possible methods to directly observe the FFLO vortex state, we discuss the NMR spectrum and FLL form factors, reflecting FFLO vortex structure. Last section is devoted to summary and discussions.

2. Quasiclassical theory including paramagnetic effect

One of the methods to study properties of superconductors by microscopic theory is a formulation of Green's functions. With field operators $\psi_\uparrow$, $\psi_\downarrow$, Green's functions are defined as

$$G(\mathbf{r},\tau;\mathbf{r}',\tau') = -\langle T_\tau[\psi_\uparrow(\mathbf{r},\tau)\psi_\uparrow^\dagger(\mathbf{r}',\tau')]\rangle,$$
$$F(\mathbf{r},\tau;\mathbf{r}',\tau') = -\langle T_\tau[\psi_\uparrow(\mathbf{r},\tau)\psi_\downarrow(\mathbf{r}',\tau')]\rangle, \quad F^\dagger(\mathbf{r},\tau;\mathbf{r}',\tau') = -\langle T_\tau[\psi_\downarrow^\dagger(\mathbf{r},\tau)\psi_\uparrow^\dagger(\mathbf{r}',\tau')]\rangle \quad (3)$$

in imaginary time formulation, where T_τ indicates time-ordering operator of τ, and $\langle\cdots\rangle$ is statistical ensemble average. The Green's functions obey Gor'kov equation derived from the BCS Hamiltonian of Eq. (1). Behaviors of Green's functions include rapid oscillation of atomic short scale at the Fermi energy. Thus, in order to solve Gor'kov equation or BdG equation for vortex structure, we need heavy calculation treating all atomic sites within a unit cell of vortex lattice. To reduce the task of the calculation, we adopt quasiclassical approximation to integrate out the rapid oscillation of the atomic scale $\sim 1/k_{\rm F}$ ($k_{\rm F}$ is Fermi wave number), and consider only the spatial variation in the length scale of the superconducting coherence length ξ_0. This is appropriate when $\xi_0 \gg 1/k_{\rm F}$, which is satisfied in most of superconductors in solid state physics. The quasiclassical Green's functions are defined as

$$g(\omega_n,\mathbf{k}_{\rm F},\mathbf{r}) = \int \frac{{\rm d}\xi}{{\rm i}\pi} G(\omega_n,\mathbf{k},\mathbf{r}),$$
$$f(\omega_n,\mathbf{k}_{\rm F},\mathbf{r}) = \int \frac{{\rm d}\xi}{\pi} F(\omega_n,\mathbf{k},\mathbf{r}), \quad f^\dagger(\omega_n,\mathbf{k}_{\rm F},\mathbf{r}) = \int \frac{{\rm d}\xi}{\pi} F^\dagger(\omega_n,\mathbf{k},\mathbf{r}), \quad (4)$$

where we consider the Fourier transformation of the Green's functions; from $\tau-\tau$ to Matsubara frequency ω_n, and from $\mathbf{r}-\mathbf{r}'$ to relative momentum $\mathbf{k}$, and integral about $\xi \equiv k^2/2m - \mu_0$, i.e., momentum directions perpendicular to the Fermi surface. Thus, the quasiclassical Green's functions depends on the momentum $\mathbf{k}_{\rm F}$ on the Fermi surface, and the center-of-mass coordinate $(\mathbf{r}+\mathbf{r}')/2 \to \mathbf{r}$.

From the Gor'kov equation, Eilenberger equations for quasiclassical Green's functions are derived as

$$\{\omega_n + \mathrm{i}\mu B + \mathbf{v}\cdot(\nabla + \mathrm{i}\mathbf{A})\} f = \Delta(\mathbf{r},\mathbf{k}_\mathrm{F}) g,$$
$$\{\omega_n + \mathrm{i}\mu B - \mathbf{v}\cdot(\nabla - \mathrm{i}\mathbf{A})\} f^\dagger = \Delta^*(\mathbf{r},\mathbf{k}_\mathrm{F}) g, \tag{5}$$

with $\mathbf{v}\cdot\nabla g = \Delta^*(\mathbf{r},\mathbf{k}_\mathrm{F}) f - \Delta(\mathbf{r},\mathbf{k}_\mathrm{F}) f^\dagger$, $g = (1 - ff^\dagger)^{1/2}$, $\mathrm{Re}g > 0$, $\Delta(\mathbf{r},\mathbf{k}_\mathrm{F}) = \Delta(\mathbf{r})\phi(\mathbf{k}_\mathrm{F})$, and $\mu = \mu_\mathrm{B} B_0/\pi k_\mathrm{B} T_\mathrm{c}$. In this chapter, length, temperature, Fermi velocity, magnetic field and vector potential are, respectively, in units of R_0, T_c, $\bar{v}_\mathrm{F}$, B_0 and $B_0 R_0$. Here, $R_0 = \hbar\bar{v}_\mathrm{F}/2\pi k_\mathrm{B} T_\mathrm{c}$ is in the order of coherence length, $B_0 = \hbar c/2|e|R_0^2$, and $\bar{v}_\mathrm{F} = \langle v_\mathrm{F}^2\rangle_{\mathbf{k}_\mathrm{F}}^{1/2}$ is an averaged Fermi velocity on the Fermi surface. $\langle\cdots\rangle_{\mathbf{k}_\mathrm{F}}$ indicates the Fermi surface average. Energy E, pair potential Δ and Matsubara frequency ω_n are in unit of $\pi k_\mathrm{B} T_\mathrm{c}$. We set the pairing function $\phi(\mathbf{k}_\mathrm{F}) = 1$ in the s-wave pairing, and $\phi(\mathbf{k}_\mathrm{F}) = \sqrt{2}(k_a^2 - k_b^2)/(k_a^2 + k_b^2)$ in the d-wave pairing. The vector potential is given by $\mathbf{A} = \frac{1}{2}\bar{\mathbf{B}}\times\mathbf{r} + \mathbf{a}$ in the symmetric gauge, with an average flux density $\bar{\mathbf{B}} = (0,0,\bar{B})$. The internal field is obtained as $\mathbf{B}(\mathbf{r}) = \bar{\mathbf{B}} + \nabla\times\mathbf{a}$.
The pair potential is selfconsistently calculated by

$$\Delta(\mathbf{r}) = g_0 N_0 T \sum_{0\le\omega_n\le\omega_\mathrm{cut}} \left\langle \phi^*(\mathbf{k}_\mathrm{F}) \left(f + f^{\dagger *}\right)\right\rangle_{\mathbf{k}_\mathrm{F}} \tag{6}$$

with $(g_0 N_0)^{-1} = \ln T + 2T\sum_{0\le\omega_n\le\omega_\mathrm{cut}} \omega_n^{-1}$. We set high-energy cutoff of the pairing interaction as $\omega_\mathrm{cut} = 20 k_\mathrm{B} T_\mathrm{c}$. The vector potential is selfconsistently determined by the paramagnetic moment $\mathbf{M}_\mathrm{para} = (0,0,M_\mathrm{para})$ and the supercurrent $\mathbf{j}_\mathrm{s}$ as

$$\nabla\times\nabla\times\mathbf{a}(\mathbf{r}) = \mathbf{j}_\mathrm{s}(\mathbf{r}) + \nabla\times\mathbf{M}_\mathrm{para}(\mathbf{r}) \equiv \mathbf{j}(\mathbf{r}), \tag{7}$$

with

$$\mathbf{j}_\mathrm{s}(\mathbf{r}) = -\frac{2T}{\kappa^2}\sum_{0\le\omega_n} \langle \mathbf{v}_\mathrm{F}\mathrm{Im}\{g\}\rangle_{\mathbf{k}_\mathrm{F}}, \tag{8}$$

$$M_\mathrm{para}(\mathbf{r}) = M_0\left(\frac{B(\mathbf{r})}{\bar{B}} - \frac{2T}{\mu\bar{B}}\sum_{0\le\omega_n}\langle \mathrm{Im}\{g\}\rangle_{\mathbf{k}_\mathrm{F}}\right). \tag{9}$$

Here, the normal state paramagnetic moment $M_0 = (\mu/\kappa)^2\bar{B}$, $\kappa = B_0/\pi k_\mathrm{B} T_\mathrm{c}\sqrt{8\pi N_0}$, N_0 is DOS at the Fermi energy in the normal state.
The unit cell of the vortex lattice is given by $\mathbf{r} = w_1(\mathbf{u}_1 - \mathbf{u}_2) + w_2\mathbf{u}_2 + w_3\mathbf{u}_3$ with $-0.5 \le w_i \le 0.5$ (i=1, 2, 3), $\mathbf{u}_1 = (a,0,0)$, $\mathbf{u}_2 = (\zeta a, a_y, 0)$ with $\zeta = 1/2$, and $\mathbf{u}_3 = (0,0,L)$. For triangular vortex lattice $a_y/a = \sqrt{3}/2$, and $a_y/a = 1/2$ for square vortex lattice. For the FFLO modulation, we assume $\Delta(x,y,z) = \Delta(x,y,z+L)$ and $\Delta(x,y,z) = -\Delta(x,y,-z)$. Then, $\Delta(\mathbf{r}) = 0$ at the FFLO nodal planes $z = 0$, and $\pm 0.5L$. These configurations of the FFLO vortex structure are schematically shown in Fig. 2, which show the unit cell in the xz plane including vortex lines, and in the xy plane. We divide w_i to N_i-mesh points in our numerical studies, and calculate the quasiclassical Green's functions, $\Delta(\mathbf{r})$, $M_\mathrm{para}(\mathbf{r})$ and $\mathbf{j}(\mathbf{r})$ at each mesh point in the three dimensional (3D) space. Typically we set $N_1 = N_2 = N_3 = 31$ for the calculation of vortex states with FFLO modulation. For the vortex states without FFLO modulation, we assume uniform structure along the magnetic field direction, and set $N_1 = N_2 = 41$.
We solve Eq. (5) for g, f, $f^\dagger$, and Eqs. (6)-(9) for $\Delta(\mathbf{r})$, $M_\mathrm{para}(\mathbf{r})$, $\mathbf{A}(\mathbf{r})$, alternately, and obtain selfconsistent solutions, by fixing a unit cell of the vortex lattice and a period L of the FFLO

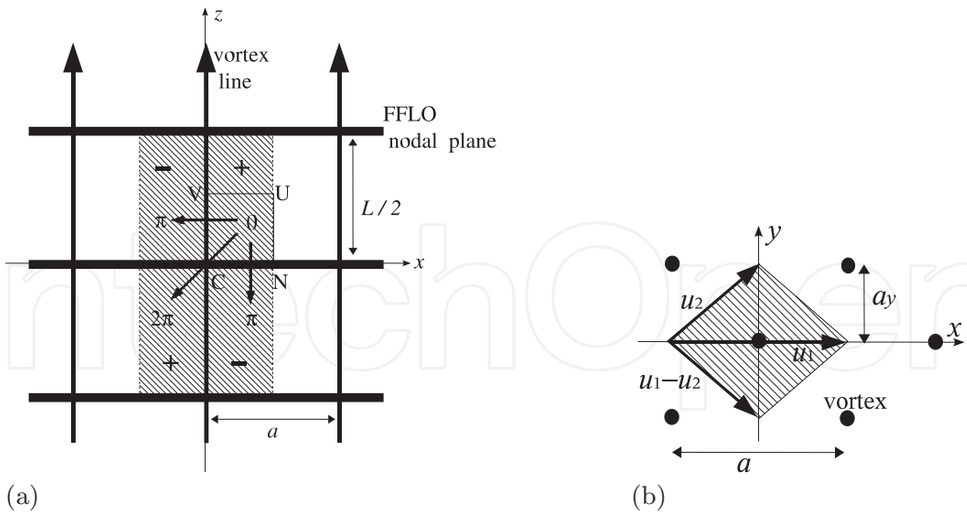

Fig. 2. Configurations of the vortex lines and the FFLO nodal planes are schematically presented in the xz plane including vortex lines (a) and in the xy plane (b). The inter-vortex distance is a in the x direction, and the distance between the FFLO nodal planes is $L/2$. The hatched region indicates the unit cell. In (a), along the trajectories presented by "$0 \longrightarrow \pi$", the pair potential changes the sign ($+ \rightarrow -$) across the vortex line or across the FFLO nodal plane, due to the π-phase shift of the pair potential. Along the trajectory presented by "$0 \longrightarrow 2\pi$", the sign of the the pair potential does not change ($+ \rightarrow +$) across the intersection point of the vortex line and the FFLO nodal plane, since the phase shift is 2π. In (b), $\bullet$ indicates the vortex center. $\mathbf{u}_1 - \mathbf{u}_2$ and $\mathbf{u}_2$ are unit vectors of the vortex lattice.

modulation. When we solve Eq. (5), we estimate $\Delta(\mathbf{r})$ and $\mathbf{A}(\mathbf{r})$ at arbitrary positions by the interpolation from their values at the mesh points, and by the periodic boundary condition of the unit cell including the phase factor due to the magnetic field. The boundary condition is given by

$$\Delta(\mathbf{r}+\mathbf{R}) = \Delta(\mathbf{r})\mathrm{e}^{\mathrm{i}\chi(\mathbf{r},\mathbf{R})} \tag{10}$$

$$\chi(\mathbf{r},\mathbf{R}) = 2\pi\{\frac{1}{2}((m+n\zeta)\frac{y}{a_y} - n\frac{x}{a_x}) + \frac{mn}{2} + (m+n\zeta)\frac{y_0}{a_y} - n\frac{x_0}{a_x}\} \tag{11}$$

for $\mathbf{R} = m\mathbf{u}_1 + n\mathbf{u}_2$ (m, n : integer), when the vortex center is located at $(x_0, y_0) - \frac{1}{2}(\mathbf{u}_1 + \mathbf{u}_2)$. In the selfconsistent calculation of $\mathbf{a}$, we solve Eq. (7) in the Fourier space $\mathbf{q}_{m_1,m_2,m_3}$, taking account of the current conservation $\nabla \cdot \mathbf{j}(\mathbf{r}) = 0$, so that the average flux density per unit cell of the vortex lattice is kept constant. The wave number $\mathbf{q}$ is discretized as

$$\mathbf{q}_{m_1,m_2,m_3} = m_1\mathbf{q}_1 + m_2\mathbf{q}_2 + m_3\mathbf{q}_3 \tag{12}$$

with integers m_i ($i = 1,2,3$), where $\mathbf{q}_1 = (2\pi/a, -\pi/a_y, 0)$, $\mathbf{q}_2 = (2\pi/a, \pi/a_y, 0)$, and $\mathbf{q}_3 = (0, 0, 2\pi/L)$. The lattice momentum is defined as $\mathbf{G}(\mathbf{q}_{m_1,m_2,m_3}) = (G_x, G_y, G_z)$ with $G_x = [N_1 \sin(2\pi m_1/N_1) + N_2 \sin(2\pi m_2/N_2)]/a$, $G_y = [-N_1 \sin(2\pi m_1/N_1) + N_2 \sin(2\pi m_2/N_2)]/2a_y$, and $G_z = N_3 \sin(2\pi m_3/N_3)/L$. We obtain the Fourier component of $\mathbf{a}(\mathbf{r})$ as $\mathbf{a}(\mathbf{q}) = \mathbf{j}'(\mathbf{q})/|\mathbf{G}|^2$, where $\mathbf{j}'(\mathbf{q}) = \mathbf{j}(\mathbf{q}) - \mathbf{G}\,(\mathbf{G}\cdot\mathbf{j}(\mathbf{q}))\,/|\mathbf{G}|^2$ ensuring the current conservation $\nabla \cdot \mathbf{j}'(\mathbf{r}) = 0$, and $\mathbf{j}(\mathbf{q})$ is the Fourier component of $\mathbf{j}(\mathbf{r})$ in Eq. (7) (Klein, 1987). The final selfconsistent solution satisfies $\nabla \cdot \mathbf{j}(\mathbf{r}) = 0$.

Using selfconsistent solutions, we calculate free energy, external field, and LDOS. In Eilenberger theory, free energy is given by

$$F = \int_{\text{unitcell}} \mathrm{d}\mathbf{r}\Big\{\kappa^2|\mathbf{B}(\mathbf{r}) - \mathbf{H}|^2 - \mu^2|B(\mathbf{r})|^2 + |\Delta(\mathbf{r})|^2(\ln T + 2T\sum_{0<\omega_n<\omega_{\text{cut}}}\omega_n^{-1}) - T\sum_{|\omega_n|<\omega_{\text{cut}}}\langle I(\mathbf{r},\mathbf{k},\omega_n)\rangle_{\mathbf{k}_\text{F}}\Big\} \tag{13}$$

with

$$I(\mathbf{r},\mathbf{k},\omega_n) = \Delta\phi f^\dagger + \Delta^*\phi^* f + (g - \frac{\omega_n}{|\omega_n|})\Big\{\frac{1}{f}\left(\omega_n + \mathrm{i}\mu B + \mathbf{v}\cdot(\nabla + \mathrm{i}\mathbf{A})\right)f + \frac{1}{f^\dagger}\left(\omega_n + \mathrm{i}\mu B + \mathbf{v}\cdot(\nabla - \mathrm{i}\mathbf{A})\right)f^\dagger\Big\}. \tag{14}$$

Using Eqs. (5) and (6), we obtain

$$F = \int_{\text{unitcell}} \mathrm{d}\mathbf{r}\Big\{\kappa^2|\mathbf{B}(\mathbf{r}) - \mathbf{H}|^2 - \mu^2|B(\mathbf{r})|^2 + T\sum_{|\omega_n|<\omega_{\text{cut}}}\mathrm{Re}\left\langle\frac{g-1}{g+1}(\Delta\phi f^\dagger + \Delta^*\phi^* f)\right\rangle_{\mathbf{k}_\text{F}}\Big\}. \tag{15}$$

Using Doria-Gubernatis-Rainer scaling (Doria et al., 1990; Watanabe et al., 2005), we obtain the relation of $\bar{B}$ and the external field H as

$$H = \left(1 - \frac{\mu^2}{\kappa^2}\right)\left(\bar{B} + \left\langle(B(\mathbf{r}) - \bar{B})^2\right\rangle_{\mathbf{r}}/\bar{B}\right) + \frac{T}{\kappa^2\bar{B}}\left\langle\sum_{0<\omega_n}\left\langle\mu B(\mathbf{r})\mathrm{Im}\{g\} + \frac{1}{2}\mathrm{Re}\left\{\frac{(f^\dagger\Delta + f\Delta^*)g}{g+1}\right\} + \omega_n\mathrm{Re}\{g-1\}\right\rangle_{\mathbf{k}_\text{F}}\right\rangle_{\mathbf{r}}, \tag{16}$$

where $\langle\cdots\rangle_{\mathbf{r}}$ indicates the spatial average. We consider the case when $\kappa = 89$ and low temperature $T/T_\text{c} = 0.1$. For two-dimensional (2D) Fermi surface, $\kappa = (7\zeta(3)/8)^{1/2}\kappa_{\text{GL}} \sim \kappa_{\text{GL}}$ (Miranović & Machida, 2003). Therefore we consider the case of typical type-II superconductors with large Ginzburg-Landau (GL) parameter. In these parameters, $|\bar{B} - H| < 10^{-4}B_0$.

When we calculate the electronic states, we solve Eq. (5) with $\mathrm{i}\omega_n \to E + \mathrm{i}\eta$. The LDOS is given by $N(\mathbf{r},E) = N_\uparrow(\mathbf{r},E) + N_\downarrow(\mathbf{r},E)$, where

$$N_\sigma(\mathbf{r},E) = N_0\langle\mathrm{Re}\{g(\omega_n + \mathrm{i}\sigma\mu B,\mathbf{k}_\text{F},\mathbf{r})|_{i\omega_n\to E+i\eta}\}\rangle_{\mathbf{k}_\text{F}} \tag{17}$$

with $\sigma = 1$ (-1) for up (down) spin component. We typically use $\eta = 0.01$, which is small smearing effect of energy by scatterings. The DOS is obtained by the spatial average of the LDOS as $N(E) = N_\uparrow(E) + N_\downarrow(E) = \langle N(\mathbf{r},E)\rangle_{\mathbf{r}}$.

3. Vortex states in superconductors with strong paramagnetic effect

In this section, we study the paramagnetic effect in vortex state without FFLO modulation. For simplicity, we consider fundamental case of isotropic Fermi surface, that is, 2D cylindrical Fermi surface with $\mathbf{k}_\text{F} = k_\text{F}(\cos\theta,\sin\theta)$ and Fermi velocity $\mathbf{v}_\text{F} = v_{\text{F}0}(\cos\theta,\sin\theta)$. Magnetic field is applied along the z direction. Even before the FFLO transition, the strong paramagnetic effect induces anomalous field dependence of some physical quantities by paramagnetic vortex core and paramagnetic pair-breaking. There are some theoretical approaches to

the study of paramagnetic effect, such as by BdG theory (Takahashi et al., 2006), or by Landau level expansion in Eilenberger theory(Adachi et al., 2005). Here, we report results of quantitative estimate by selfconsistent Eilenberger theory given in previous section (Ichioka & Machida, 2007).

3.1 Field dependence of paramagnetic susceptibility and zero-energy DOS

First, we discuss the field dependence of zero-energy DOS $\gamma(H) = N(E = 0)/N_0$ and paramagnetic susceptibility $\chi(H) = \langle M_{\rm para}(\mathbf{r})\rangle_{\mathbf{r}}/M_0$, which are normalized by the normal state values. From low temperature specific heats C, we obtain $\gamma(H) \propto C/T$ experimentally. And $\chi(H)$ is observed by the Knight shift in NMR experiments, which measure the paramagnetic component via the hyperfine coupling between a nuclear spin and conduction electrons. As shown in Fig. 3, γ (dashed lines) and χ (solid lines) show almost the same behavior at low temperatures. First, we see the case of d-wave pairing with line nodes in Fig. 3(a). There $\gamma(H)$ and $\chi(H)$ describe $\sqrt{H}$-like recovery smoothly to the normal state value ($\gamma = \chi = 1$ at H_{c2}) in the case of negligible paramagnetic effect ($\mu = 0.02$). With increasing the paramagnetic parameter μ, H_{c2} is suppressed and the Volovik curve $\gamma(H) \propto \sqrt{H}$ gradually changes into curves with a convex curvature. For large μ, H_{c2} changes to first order phase transition. We note that at lower fields all curves exhibit a $\sqrt{H}$ behavior because the paramagnetic effect ($\propto H$) is not effective. Further increasing H, $\gamma(H)$ behaves quite differently. There we find a turning point field which separates a concave curve at lower H and a convex curve at higher H. H/H_{c2} at the inflection point increases as μ decreases. From these behaviors, we can estimate the strength of the paramagnetic effect, μ.

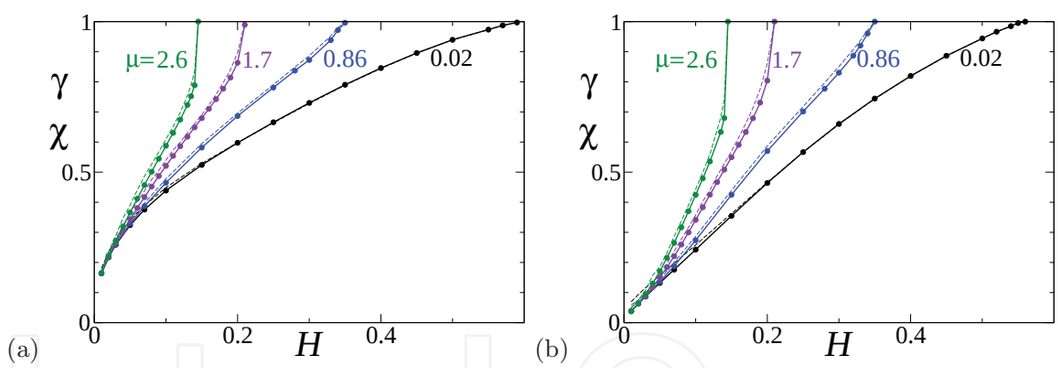

Fig. 3. The magnetic field dependence of paramagnetic susceptibility $\chi(H)$ (solid lines) and zero-energy DOS $\gamma(H)$ (dashed lines) at $T = 0.1T_c$ for various paramagnetic parameters $\mu = 0.02$, 0.86, 1.7, and 2.6 in the d-wave (a) and s-wave (b) pairing cases.

To examine effects of the pairing symmetry, we show $\gamma(H)$ and $\chi(H)$ also for s-wave pairing in Fig. 3(b). In the H-dependence of $\gamma(H)$ and $\chi(H)$, differences by the vortex lattice configuration of triangular or square are negligibly small. The difference in the H-dependences of Figs. 3(a) and 3(b) at low fields comes from the gap structure of the pairing function. In the full gap case of s-wave pairing, $\gamma(H)$ and $\chi(H)$ show H-linear-like behavior at low fields. With increasing the paramagnetic effect, H-linear behaviors gradually change into curves with a convex curvature. As seen in Figs. 3(a) and 3(b), paramagnetic effects appear similarly at high fields both for s-wave and d-wave pairings.

The H-dependence of $\gamma(H)$ for $H \parallel c$ and $H \parallel ab$ was used to identify the pairing symmetry and paramagnetic effect in URu_2Si_2 (Yano et al., 2008).

3.2 Field dependence of magnetization

We discuss the paramagnetic effect on the magnetization curves. The magnetization $M_{\text{total}} = \bar{B} - H$ includes both the diamagnetic and the paramagnetic contributions. In Fig. 4, magnetization curves are presented as a function of H for various μ at $T = 0.1T_{\text{c}}$ for s-wave and d-wave pairings. When the paramagnetic effect is negligible, we see typical magnetization curve of type-II superconductors. There, $|M_{\text{total}}|$ in s-wave pairing is larger, compared with that in d-wave pairing. Dashed lines in Fig. 4 indicate the magnetization in normal states, which shows linear increase of paramagnetic moments as a function of magnetic fields. When paramagnetic effect is strong for large μ, $M_{\text{total}}(H)$ exhibits a sharp rise near H_{c2} by the paramagnetic pair breaking effect, and that $M_{\text{total}}(H)$ has convex curvature at higher fields, instead of a conventional concave curvature. These behaviors are qualitatively seen in experimental data of $CeCoIn_5$ (Tayama et al., 2002).

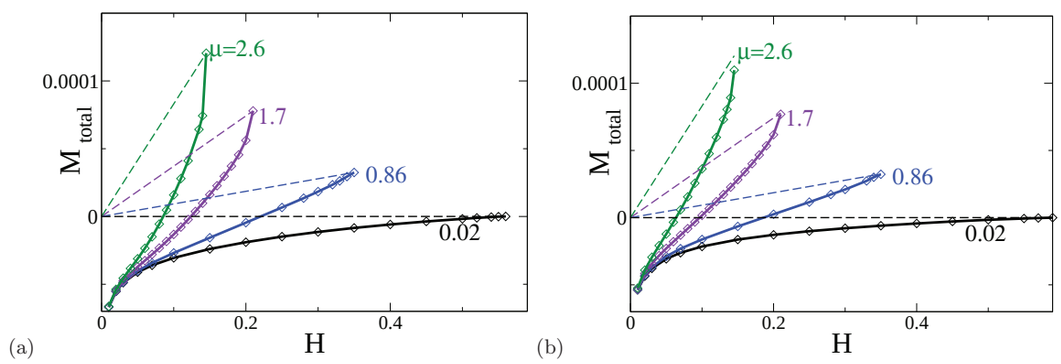

Fig. 4. Magnetization curve M_{total} as a function of H at $T/T_{\text{c}} = 0.1$ for $\mu = 0.02, 0.86, 1.7$ and 2.6 in s-wave (a) and d-wave (b) pairings. Dashed lines are normal state magnetization.

In Fig. 5(a), magnetization curves are presented as a function of H for various T at $\mu = 1.7$. With increasing T, the rapid increase of $M_{\text{total}}(H)$ near H_{c2} is smeared. In Fig. 5(b), M_{total} is plotted as a function of T^2 for various $\bar{B}$. We fit these curves as $M_{\text{total}}(T, H) = M_0 + \frac{1}{2}\beta(H)T^2 + O(T^3)$ at low T. The slope $\beta(H) = \lim_{T\to 0} \partial^2 M_{\text{total}}/\partial T^2$ decreases on raising H at lower fields. However, at higher fields approaching H_{c2}, the slope $\beta(H)$ sharply increases. Thus, as shown in Fig. 5(c), $\beta(H)$ as a function of H exhibits a minimum at intermediate H and rapid increase near H_{c2} by the paramagnetic effect when $\mu = 1.7$. This is contrasted with the case of negligible paramagnetic effect ($\mu = 0.02$), where $\beta(H)$ is a decreasing function of H until H_{c2}. The behavior of $\beta(H)$ is consistent with that of $\gamma(H)$, since there is a relation $\beta(H) \propto \partial\gamma(H)/\partial H$ obtained from a thermodynamic Maxwell's relation $\partial^2 M_{\text{total}}/\partial T^2 = \partial(C/T)/\partial B$ and $B \sim H$ (Adachi et al., 2005). In Fig. 3, we see that for $\mu = 1.7$ the slope of $\gamma(H)$ is decreasing function of H at low H, but changes to increasing function near H_{c2}. This behavior correctly reflects the H-dependence of $\beta(H)$.

3.3 Paramagnetic contribution on vortex core structure

In order to understand contributions of the paramagnetic effect on the vortex structure, we illustrate the local structures of the pair potential $|\Delta(\mathbf{r})|$, paramagnetic moment $M_{\text{para}}(\mathbf{r})$, and internal magnetic field $B(\mathbf{r})$ within a unit cell of the vortex lattice in Fig. 6. Since we assume d-wave pairing with the line node gap here, the vortex core structure is deformed to fourfold symmetric shape around a vortex core (Ichioka et al., 1999a;b; 1996). It is noted that the paramagnetic moment is enhanced exclusively around the vortex core, as shown in Fig. 6(b). Since the contribution of the paramagnetic vortex core is enhanced with increasing

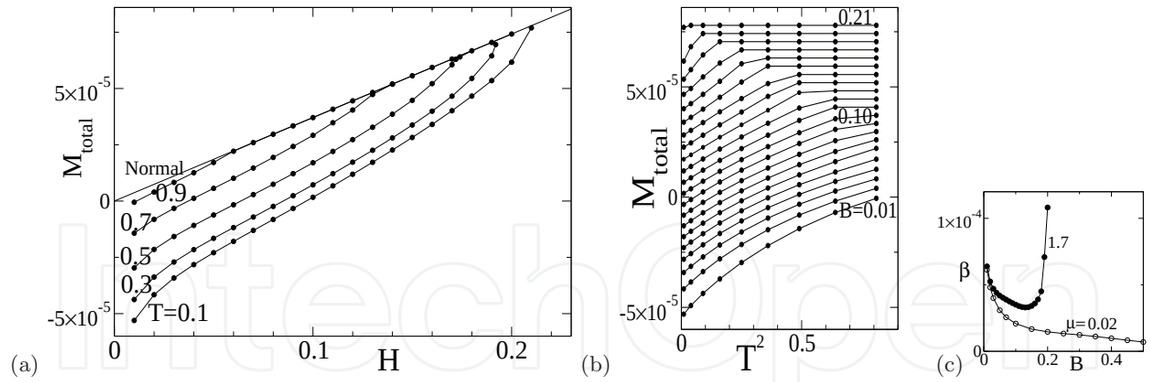

Fig. 5. (a) Magnetization curve M_{total} as a function of H for $\mu = 1.7$ at $T/T_c = 0.1$, 0.3, 0.5, 0.7, 0.9 and 1.0 (normal state) in d-wave pairing. (b) M_{total} as a function of T^2 at $H = 0.01$, 0.02, 0.03, $\cdots$, 0.21. (c) H-dependence of factor $\beta(H)$ at $\mu = 0.02$ and 1.7.

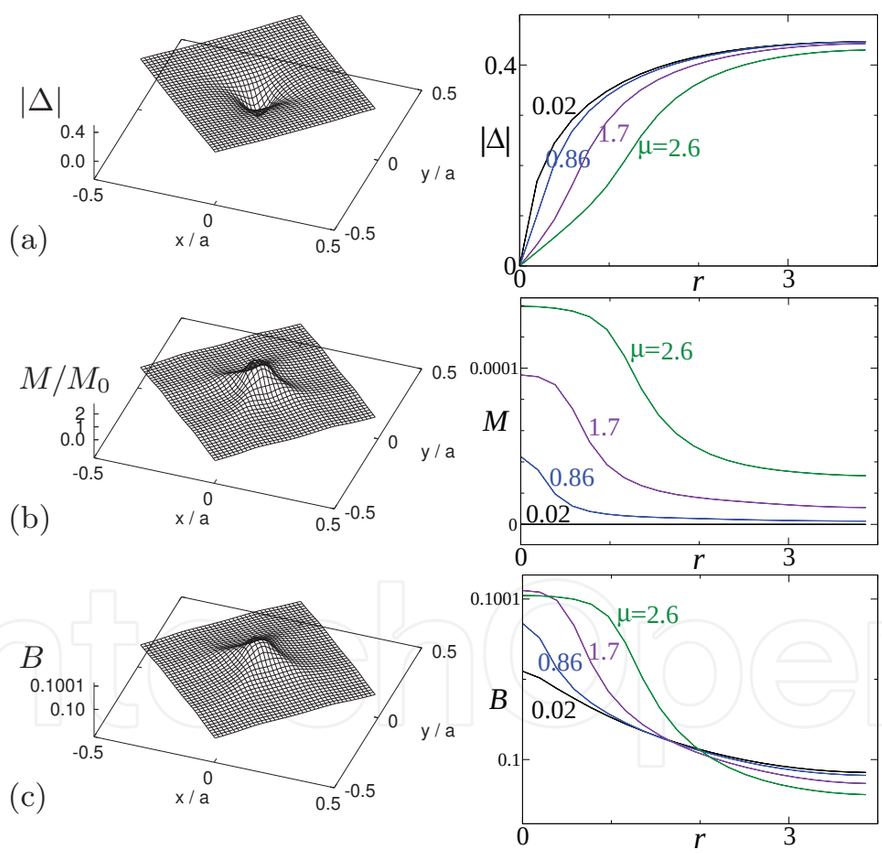

Fig. 6. Spatial structure of the pair potential (a), paramagnetic moment (b) and internal magnetic field (c) at $T = 0.1T_c$ and $H \sim \bar{B} = 0.1B_0$, where $a = 11.2R_0$, in d-wave pairing. The left panels show $|\Delta(\mathbf{r})|$, $M_{\text{para}}(\mathbf{r})$, and $B(\mathbf{r})$ within a unit cell of the square vortex lattice at $\mu = 1.7$. The right panels show the profiles along the trajectory r from the vortex center to a midpoint between nearest neighbor vortices. $\mu = 0.02$, 0.86, 1.7, and 2.6.

μ, internal field $B(\mathbf{r})$ consisting of diamagnetic and paramagnetic contributions is further enhanced around the vortex core by the paramagnetic effect, as shown in Fig. 6(c). When μ is large, the pair potential $|\Delta(\mathbf{r})|$ is slightly suppressed around the paramagnetic vortex core, and the vortex core radius is enlarged, as shown in Fig. 6(a).

The enhancement of $M_{\text{para}}(\mathbf{r})$ around vortex core is related to spatial structure of the LDOS $N_\sigma(\mathbf{r}, E)$. As shown in Fig. 7(a), the LDOS spectrum shows *zero-energy peak* at the vortex center, but the spectrum is shifted to $E = \pm\mu H$ due to Zeeman shift. There is a relation between the LDOS spectrum and local paramagnetic moment, as

$$M_{\text{para}}(\mathbf{r}) = -\mu_{\text{B}} \int_{-\infty}^{0} \{N_\uparrow(E, \mathbf{r}) - N_\downarrow(E, \mathbf{r})\} \mathrm{d}E. \tag{18}$$

In Fig. 7(a), the peak states at $E > 0$ is empty for $N_\uparrow(E, \mathbf{r})$, and the peak at $E < 0$ is occupied for $N_\downarrow(E, \mathbf{r})$. Therefore, because of Zeeman shift of the zero-energy peak at the vortex core, large $M_{\text{para}}(\mathbf{r})$ appears due to the local imbalance of up- and down-spin occupation around the vortex core. As shown in Figs. 7(b) and 7(c), moving from the vortex center to outside, the peak of the spectrum is split into two peaks, which are shifted to higher and lower energies, respectively. When one of split peaks crosses $E = 0$, the imbalance of up- and down-spin occupation is decreased. Thus, $M_{\text{para}}(\mathbf{r})$ is suppressed outside of vortex cores. This corresponds to the behavior of Knight shift, i.e., the paramagnetic moment is suppressed in uniform states of spin-singlet pairing superconductors by the formation of Cooper pair between spin-up and spin-down electrons.

In Figs. 7(d) and 7(e), we present the spectrum of spatially-averaged DOS. In the DOS spectrum, peaks of the LDOS are smeared by the spatial average. Because of the flat spectrum at low energies, paramagnetic susceptibility $\chi(H)$ shows almost the same H-behavior as the zero-energy DOS $\gamma(H) \sim N(E = 0)$ even for large μ, as shown in Fig. 3, while $\chi(H)$ counts the DOS contribution in the energy range $|E| < \mu H$, i.e., from Eq. (18),

$$\chi(H) \sim \int_0^{\mu H} N_\uparrow(E) \mathrm{d}E / \mu H. \tag{19}$$

3.4 Field dependence of flux line lattice form factor

One of the best ways to directly see the accumulation of the paramagnetic moment around the vortex core is to observe the Bragg scattering intensity of the FLL in SANS experiment. The intensity of the (h, k)-diffraction peak is given by $I_{h,k} = |F_{h,k}|^2/|\mathbf{q}_{h,k}|$ with the wave vector $\mathbf{q}_{h,k} = h\mathbf{q}_1 + k\mathbf{q}_2$, $\mathbf{q}_1 = (2\pi/a, -\pi/a_y, 0)$ and $\mathbf{q}_2 = (2\pi/a, \pi/a_y, 0)$. The Fourier component $F_{h,k}$ is given by $B(\mathbf{r}) = \sum_{h,k} F_{h,k} \exp(\mathrm{i}\mathbf{q}_{h,k} \cdot \mathbf{r})$. In the SANS for FLL observation, the intensity of the main peak at $(h, k) = (1, 0)$ probes the magnetic field contrast between the vortex cores and the surrounding.

The field dependence of $|F_{1,0}|^2$ in our calculations is shown in Fig. 8(a). In the case of negligible paramagnetic effect ($\mu = 0.02$), $|F_{1,0}|^2$ decreases exponentially as a function of H. This exponential decay is typical behavior of conventional superconductors. With increasing paramagnetic effect, however, the decreasing slope of $|F_{1,0}|^2$ becomes gradual, and changes to increasing functions of H at lower fields in strong paramagnetic case ($\mu = 2.6$).

The reason of anomalous enhancement of $|F_{1,0}|$ at high fields is because $|F_{1,0}|$ reflects the enhanced internal field around the vortex core, shown in Fig. 6(c), by the induced paramagnetic moment at the core. We present H-dependence of $|F_{1,0}|$ with the paramagnetic contribution $|M_{1,0}|$ in Fig. 8(b). Fourier component $M_{1,0}$ is calculated from paramagnetic

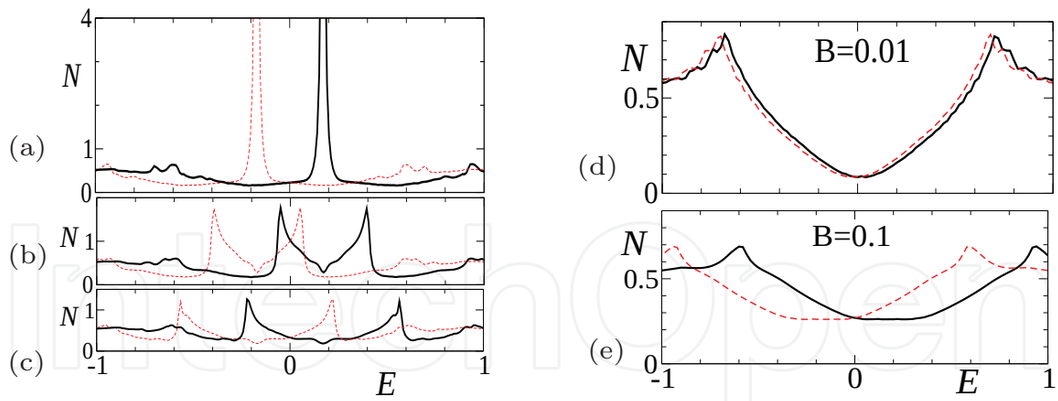

Fig. 7. Local density of states at $r/R_0 = 0$ (a), 0.8 (b) and 1.6 (c) from the vortex center towards the nearest neighbor vortex direction in d-wave pairing. Solid lines show $N_\uparrow(\mathbf{r}, E)/N_0$ for up-spin electrons, and dashed lines show $N_\downarrow(\mathbf{r}, E)/N_0$ at $H = 0.1B_0$. $\mu = 1.7$ and $T = 0.1T_c$. Spatial-averaged DOS at $H/B_0 = 0.01$ (d) and 0.1 (e) in d-wave pairing. Solid lines show $N_\uparrow(E)/N_0$ for up-spin electrons, and dashed lines show $N_\downarrow(E)/N_0$.

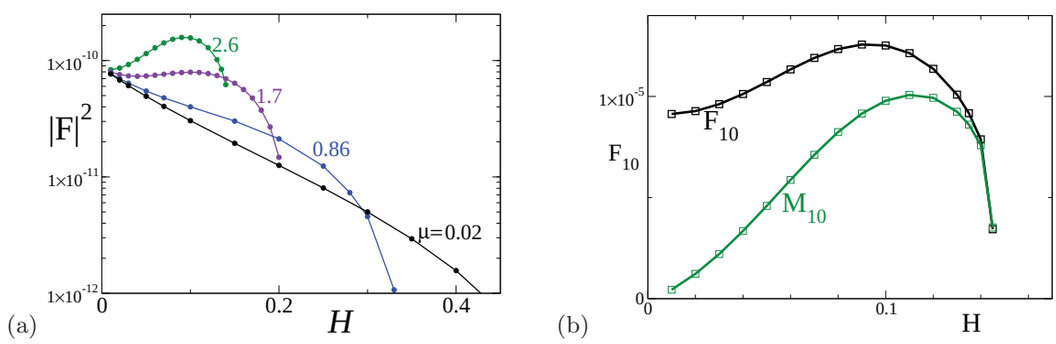

Fig. 8. Field dependence of FLL form factor $F_{1,0}$ for $\mu = 0.02$, 0.86, 1.7, and 2.6 at $T = 0.1T_c$ in d-wave pairing. (a) $|F_{1,0}|^2$ is plotted as a function of H. The vertical axis is in logarithmic scale. (b). Field dependence of $|F_{1,0}|$ and the paramagnetic contribution $|M_{1,0}|$ for $\mu = 2.6$. The vertical axis is in linear scale.

moment $M_{\text{para}}(\mathbf{r})$. From Fig. 8(b), we see that the increasing behavior of $|F_{1,0}|$ is due to the paramagnetic contribution $M_{1,0}$ proportional to μH. In Fig. 9, we present how profiles of $M_{\text{para}}(\mathbf{r})$ and $B(\mathbf{r})$ change, depending on magnetic fields. The form factors $|F_{1,0}|$ and $|M_{1,0}|$ reflect the contrast of the variable range in the figures. Increasing magnetic field at low fields ($H = 0.02, 0.06$), $M_{\text{para}}(\mathbf{r})$ is enhanced at vortex core. Reflecting this, $B(\mathbf{r})$ is also enhanced at the core, and the form factor $|F_{1,0}|$ increases as a function of a magnetic field. At higher fields ($H = 0.10, 0.12, 0.14$), inter-vortex distance becomes short. Because of overlap of the regions around vortex core with those of neighbor vortices, the contrasts of enhanced $M_{\text{para}}(\mathbf{r})$ and $B(\mathbf{r})$ around vortex core are smeared. Therefore, form factors $|F_{1,0}|$ and $|M_{1,0}|$ decrease at high fields near H_{c2} in Fig. 8(b).

The SANS experiment in $CeCoIn_5$ for $H \parallel c$ reported that $|F_{1,0}|^2$ increases until near H_{c2} instead of exponential decay (Bianchi et al., 2008; DeBeer-Schmitt et al., 2006; White et al., 2010). The anomalous increasing H-dependence of the SANS intensity in $CeCoIn_5$ can be explained qualitatively by the strong paramagnetic effect, as shown by our calculation. The detailed comparison with the experimental data will be discussed later. Anomalous

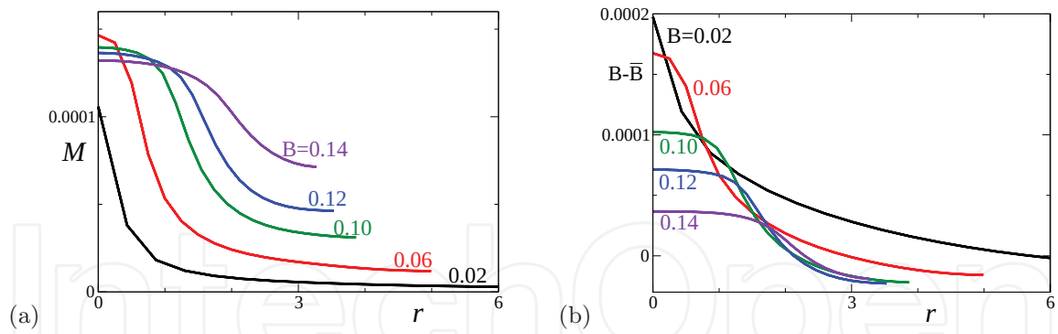

Fig. 9. Profile of paramagnetic moment $M_{\rm para}(\mathbf{r})$ (a) and internal field $B(\mathbf{r}) - \bar{B}$ (b) as a function of radius r until a midpoint between vortices along nearest neighbor vortex directions. $\mu = 2.6$ and $H = 0.02$, 0.06, 0.10, 0.12 and 0.14.

enhancement of FLL form factor was also observed in $TmNi_2B_2C$, and explained by effective strong paramagnetic effect (DeBeer-Schmitt et al., 2007).

3.5 Comparison with experimental data in $CeCoIn_5$

Here, we discuss anomalous field dependence of low T specific heat, magnetization curve, and FFL form factor in $CeCoIn_5$, based on the comparison with theoretical estimates of strong paramagnetic effect by Eilenberger theory. In Fig. 10(a), we present H-dependence of zero-energy DOS $N(E=0)$ and low-T specific heat (Ikeda et al., 2001). Both H-dependences show rapid increase at higher H. However, we see quantitative differences between theory (line A) and experimental data (circles). Compared to the theoretical estimates, C/T by experiments is smaller at low H and increase more rapidly at higher H. In order to quantitatively reproduce the H-dependence of C/T, we phenomenologically introduce factor $N_0(H)$ coming from the H-dependence of normal state DOS. So far, N_0 was assumed to be a constant in theoretical calculation. Thus, in calculation of Fermi surface average, we modify $\langle\cdots\rangle_{\mathbf{k}_F} \to \langle\cdots\rangle_{\mathbf{k}_F} N_0(H)/N_0(H_{c2})$. As shown in Fig. 10(a), the H-dependence of C/T can be reproduced, if we set $N_0(H)/N_0(H_{c2}) = 1 - 0.53\{\tanh 4(1 - H/H_{c2})\}^3$. This expression of $N_0(H)$ is phenomenological one to reproduce the experimental behavior, without microscopic theoretical consideration. This H-dependence of $N_0(H)$ indicates that normal states DOS is enhanced near H_{c2}, and may be related to the effective mass enhancement near QCP (Bianchi, Movshovich, Vekhter, Pagliuso & Sarrao, 2003; Paglione et al., 2003), which is suggested to exist at $H_{c2}(T=0)$ in $CeCoIn_5$.

Theoretical and experimental (Tayama et al., 2002) magnetization curve is presented in Fig. 10(b). There we see rapid increase at high fields and jump at H_{c2} by strong paramagnetic effects. The differences between experimental data (average of magnetization curves for increasing and decreasing H) and theoretical estimate with constant N_0 (line A) are improved by considering the H-dependence of $N_0(H)$ (line B). There, by $N_0(H)$, slope of $M_{\rm total}(H)$ becomes similar to that of experimental curve.

The H-dependence of FLL form factors using $N_0(H)$ is presented in Fig. 11. There, $|F_{1,0}|^2$ shows further increases until higher H. This sharp peak at high fields resembles to the anomalous increasing behavior observed by SANS experiment in $CeCoIn_5$ (Bianchi et al., 2008; DeBeer-Schmitt et al., 2006). For higher T, the peak is smeared and the peak position is shifted to lower fields. This T-dependence is consistent to those in experimental observation in $CeCoIn_5$ (White et al., 2010).

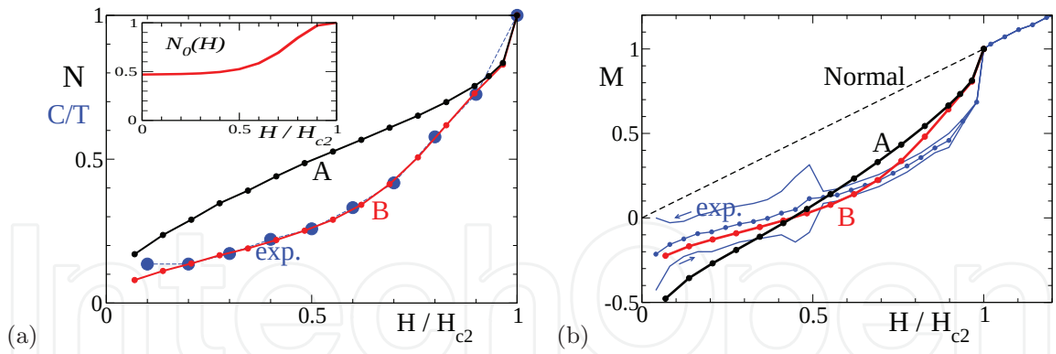

Fig. 10. (a) H-dependence of theoretical estimate (lines) for $N(E=0)$, and experimental data (Ikeda et al., 2001) of low-T specific heat C/T (circles). Line A is an original estimate for constant N_0. For line B, we assume $N_0(H)/N_0(H_{c2}) = 1 - 0.53\{\tanh 4(1 - H/H_{c2})\}^3$. Inset shows $N_0(H)/N_0(H_{c2})$ as a function of H/H_{c2}. (b) Magnetization curve $M_{\text{total}}(H)$ for constant N_0 (line A), and for $N_0(H)$ (line B). Experimental magnetization curves for increasing H(line with right arrow), decreasing H (line with left arrow), and their average (line with dots) are presented (Tayama et al., 2002). We compare the average line with lines A and B.

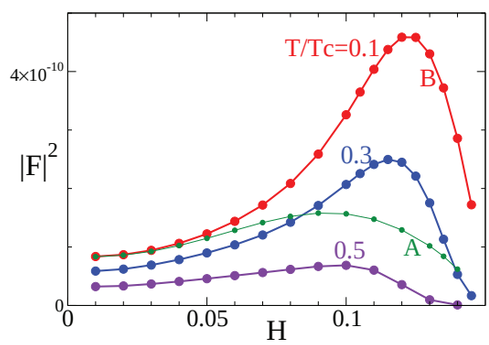

Fig. 11. H-dependence of FLL form factor $|F_{10}|^2$ at $T/T_c = 0.1$ (line B), 0.3, and 0.5 for $N_0(H)$. The line A is for constant N_0 and $T = 0.1T_c$. $\mu = 2.6$.

The above phenomenological discussion by $N_0(H)$ indicates that anomalous H-dependences observed in $CeCoIn_5$ is qualitatively reproduced by theoretical estimate considering strong paramagnetic effect, but they still show systematic quantitative deviations from theoretical estimate. These indicate that we need to consider additional effect, such as effective mass enhancement near QCP, in addition to strong paramagnetic effect, in order to understand anomalous H-dependence in $CeCoIn_5$.

4. Fulde-Ferrell-Larkin-Ovchinnikov (FFLO) vortex state

The FFLO state (Fulde & Ferrell, 1964; Larkin & Ovchinnikov, 1965) is an exotic superconducting state expected to appear at low temperatures and high fields, when the paramagnetic effect due to the Zeeman shift is significant. In the FFLO state, since the Fermi surfaces for up-spin and down-spin electron bands are split by the Zeeman shift, Cooper pairs of up- and down-spins acquire non-zero momentum for the center of mass coordinate of the Cooper pair, inducing the spatial modulation of the pair potential. The possible FFLO state is widely discussed in various research fields, ranging from superconductors in condensed

matters, neutral Fermion superfluids in an atomic cloud (Machida et al., 2006; Partridge et al., 2006; Zwierlein et al., 2006), to color superconductivity in high energy physics (Casalbuoni & Nardulli, 2004).

Experimentally, the FFLO state is suggested in a high field phase of a quasi-two dimensional (Q2D) heavy Fermion superconductor $CeCoIn_5$ for $H \parallel ab$ and $H \parallel c$ (Bianchi, Movshovich, Capan, Pagliuso & Sarrao, 2003; Radovan et al., 2003), as reviewed by Matsuda & Shimahara (2007). There, it is supposed that nodal planes of the pair potential run perpendicular to the vortex lines. For $H \parallel ab$, since spin density wave (SDW) appears in the high-field phase (Kenzelmann et al., 2010; 2008; Koutroulakis et al., 2010; Young et al., 2007), we are interested in the relation of FFLO and SDW.

In theoretical studies, many calculations for the FFLO states have been done by neglecting vortex structure. However, we have to consider the vortex structure in addition to the FFLO modulation, because the FFLO state appears at high fields in the mixed states. Among the FFLO states, there are two possible spatial modulation of the pair potential Δ. One is the Fulde-Ferrell (FF) state (Fulde & Ferrell, 1964) with phase modulation such as $\Delta \propto e^{iqz}$, where q is the modulation vector of the FFLO states. The other is the Larkin-Ovchinnikov (LO) state (Larkin & Ovchinnikov, 1965) with the amplitude modulation such as $\Delta \propto \sin qz$, where the pair potential shows periodic sign change, and $\Delta = 0$ at the nodal planes. We discuss the case of the LO states in this section, since some experimental (Matsuda & Shimahara, 2007) and theoretical (Houzet & Buzdin, 2001; Ikeda & Adachi, 2004) works support the LO state for the FFLO states in $CeCoIn_5$. In the FFLO vortex state, it is instructive to clarify the role of the FFLO nodal plane in order to obtain clear evidence of the FFLO states among the experimental data.

When we consider vortex structure in the LO state, there are two possible choices of the configuration for the vortex lines and the FFLO modulation. That is, the modulation vector of the FFLO state is parallel (Tachiki et al., 1996) or perpendicular (Klein et al., 2000; Shimahara, 1994) to the applied magnetic field. In our study, 3D structure of the former case is investigated by the selfconsistent Eilenberger theory. We calculate the spatial structures of pair potentials, paramagnetic moments, internal magnetic fields and electronic states in the vortex lattice state with the FFLO modulation. In our study, fully 3D structures of the vortex and the FFLO modulation are determined by the selfconsistent calculation with local electronic states. Since we can consider the system of vortex lattice and periodic FFLO modulation by the periodic boundary condition, we can discuss the overlaps between tails of the neighbor vortex cores or FFLO nodal planes. These calculations for the periodic systems make us possible to estimate the resonance line shapes in the NMR experiments and FLL form factors in SANS experiments.

On the other hand, the vortex and FFLO nodal plane structures in the FFLO state were calculated by the BdG theory for a single vortex in a superconductor under a cylindrical symmetry situation (Mizushima et al., 2005b). This study clarifies that the topological structure of the pair potential plays important roles to determine the electronic structures in the FFLO vortex state. The pair potential has 2π-phase winding around the vortex line, and π-phase shift at the nodal plane of the FFLO modulation. These topologies of the pair potential structure affect the distribution of paramagnetic moment and low energy electronic states inside the superconducting gap. For example, the paramagnetic moment is enhanced at the vortex core and the FFLO nodal plane. These structures are related to the bound states due to the π-phase shift of the pair potential.

In this section, we report our study of FFLO vortex states for a fundamental case of s-wave pairing and 3D spherical Fermi surface, where $\mathbf{k}_{\mathrm{F}} = k_{\mathrm{F}}(\sin\theta\cos\phi, \sin\theta\sin\phi, \cos\theta)$ and Fermi velocity $\mathbf{v}_{\mathrm{F}} = v_{\mathrm{F0}}(\sin\theta\cos\phi, \sin\theta\sin\phi, \cos\theta)$. The calculations of FFLO vortex states for Q2D Fermi surface with rippled cylinder-shape and $H \parallel ab$ both for s-wave and d-wave pairings were reported elsewhere (Ichioka et al., 2007). Main characteristic properties of FFLO vortex state do not seriously depend on the pairing symmetry.

4.1 Spatial structure of FFLO vortex states

In the left panels of Fig. 12, we show the spatial structure of the FFLO vortex state within a unit cell in the slice of the xz plane, i.e., the hatched region shown in Fig. 2(a). Right panels of Fig. 12 are for profiles of the spatial structure along the path UNCVU shown in Fig. 2(a). The point C ($x = y = z = 0$) is the intersection point of a vortex and a nodal plane. The point V ($x = y = 0$, $z = L/4$) is at the vortex center and far from the FFLO nodal plane. The point N ($x = a/2$, $y = z = 0$) is at the FFLO nodal plane and outside of the vortex. The point U ($x = a/2$, $y = 0$, $z = L/4$) is far from both the vortex and the FFLO nodal plane.

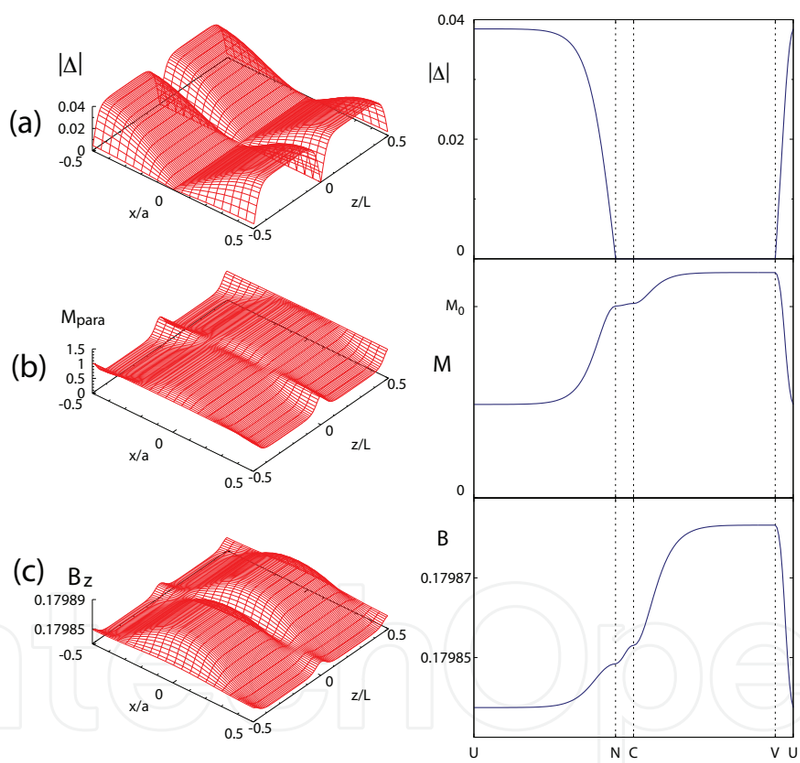

Fig. 12. Spatial structure of the FFLO vortex state in the xz plane at $\bar{B} = 0.17985B_0$, $T = 0.2T_{\mathrm{c}}$ and $L = 100R_0$ for the s-wave pairing and spherical Fermi surface. (a) Amplitude of the pair potential $|\Delta(\mathbf{r})|$. (b) Paramagnetic moment $M_{\mathrm{para}}(\mathbf{r})$. (c) Internal magnetic field $B_z(\mathbf{r})$. The left panels show the spatial variation within a unit cell, i.e., hatched region in Fig. 2(a). The right panels present the profiles along the path UNCVU shown in Fig. 2(a).

In the left panel of Fig. 12(a), we show the amplitude of the order parameter, $|\Delta(\mathbf{r})|$, which is suppressed near the vortex center at $x = y = 0$ and the FFLO nodal plane at $z = 0, \pm 0.5L$. Far from the FFLO nodal plane such as $z = 0.25L$ [along path VU], $|\Delta(\mathbf{r})|$ shows a typical profile of the conventional vortex. When we cross the vortex line or the FFLO nodal plane, the sign

of $\Delta(\mathbf{r})$ changes due to the π-phase shift of the pair potential as schematically shown in Fig. 2(a). In the profile of $|\Delta(\mathbf{r})|$ presented in the right panels of Fig. 12(a), $|\Delta(\mathbf{r})| = 0$ along the FFLO nodal plane NC and along the vortex line CV.

Correspondingly, paramagnetic moment $M_{\rm para}(\mathbf{r})/M_0$ is presented in Fig. 12(b). The paramagnetic moment is suppressed, as Knight shift, at uniform-Δ region in the spin-singlet pairing superconductors. In the figures, we see that $M_{\rm para}(\mathbf{r})$ is suppressed outside of vortex core and far from the FFLO nodal plane, as expected. However, $M_{\rm para}(\mathbf{r})$ is enhanced at the vortex core or at the FFLO nodal plane. The reason for these structures of $M_{\rm para}(\mathbf{r})$ is discussed later in connection with the LDOS. At the FFLO nodal plane $M_{\rm para}(\mathbf{r}) \sim M_0$ [path NC in Fig. 12(b)]. Along the vortex line, $M_{\rm para}(\mathbf{r})$ is enhanced more than M_0 far from the FFLO nodal planes [position V in Fig. 12(b)].

Figure 12(c) presents the z-component of the internal field, $B_z(\mathbf{r})$. Due to the contribution of the enhanced $M_{\rm para}(\mathbf{r})$, $B_z(\mathbf{r})$ is enhanced at the FFLO nodal plane even outside of the vortex. A part of the contributions by $M_{\rm para}(\mathbf{r})$ is compensated by the diamagnetic contribution, because the average flux density per unit cell of the vortex lattice in the xy plane should conserve along the magnetic field direction. Therefore, due to the conservation, the enhancement of $B_z(\mathbf{r})$ at the FFLO nodal plane [path NC in Fig. 12(c)] is smaller, compared with the enhancement of $M_{\rm para}(\mathbf{r})$ at the FFLO nodal plane [path NC in Fig. 12(b)]. While $B_z(\mathbf{r})$ is largely enhanced than $\bar{B}$ at the vortex core far from the FFLO nodal plane [position V in Fig. 12(c)], $B_z(\mathbf{r})$ is not largely enhanced at the vortex core in the FFLO nodal plane [position C]. Therefore $B_z(\mathbf{r}) \sim \bar{B}$ at the FFLO nodal plane [path NC].

To estimate magnetic field range where the FFLO vortex state is stable, and the FFLO wave number $q = 2\pi/L$, we present the field dependence of the free energy F for some L in Fig. 13(a). At $H < 0.9987H_{\rm c2}$ conventional Abrikosov vortex state with $q = 0$ is stable, but $H > 0.9987H_{\rm c2}$ FFLO vortex state with finite q becomes stable. This is an estimate in the presence of vortices in addition to FFLO modulation. At higher H, q increases for stable FFLO state, as shown in Fig. 13(b), which indicates that the FFLO period L becomes shorter at higher H. In Figs. 13(c) and 13(d), respectively, we present profiles of $\Delta(\mathbf{r})$ and $M_{\rm para}(\mathbf{r})$ along the z-direction at a midpoint between vortices, i.e., along a line thorough UN in Fig. 2(a). When L is longer at lower H, the FFLO vortex states have wide region of constant $|\Delta(\mathbf{r})|$ and $M_{\rm para}(\mathbf{r})$. They change only near the FFLO nodal plane, where $\Delta(\mathbf{r})$ has sign change and $M_{\rm para}(\mathbf{r})$ locally accumulates as in soliton structure. On the other hand, when L becomes shorter at higher H, the region near FFLO nodal plane overlaps with that of neighbor nodal planes. Thus, both $|\Delta(\mathbf{r})|$ and $M_{\rm para}(\mathbf{r})$ become spatial structure of sinusoidal wave along z-directions.

Due to the presence of FFLO vortex states at high fields, instead of conventional Abrikosov vortex state, $H_{\rm c2}$ to normal state [$F = 0$ in Fig. 13(a)] is enhanced. We note that the FFLO vortex state is stable only in narrow H range near $H_{\rm c2}$ at $T = 0.2T_{\rm c2}$ and $\mu = 2$ for spherical Fermi surface. At lower T or for larger paramagnetic parameter μ, the FFLO vortex states becomes stable in wider H-range.

4.2 Electronic structure in the FFLO vortex state

The LDOS spectrum for up- and down-spin electrons are presented at some positions in Fig. 14. In the quasiclassical theory, $N_\sigma(E, \mathbf{r})$ are symmetric by $E \leftrightarrow -E$ in the absence of the paramagnetic effect ($\mu = 0$). In the presence of the paramagnetic effect, the LDOS spectrum for up- (down-) spin electrons is shifted to positive (negative) energy by μH due to the Zeeman shift. In this case, we have a relation $N_\uparrow(E, \mathbf{r}) = N_\downarrow(-E, \mathbf{r})$ within the quasiclassical theory.

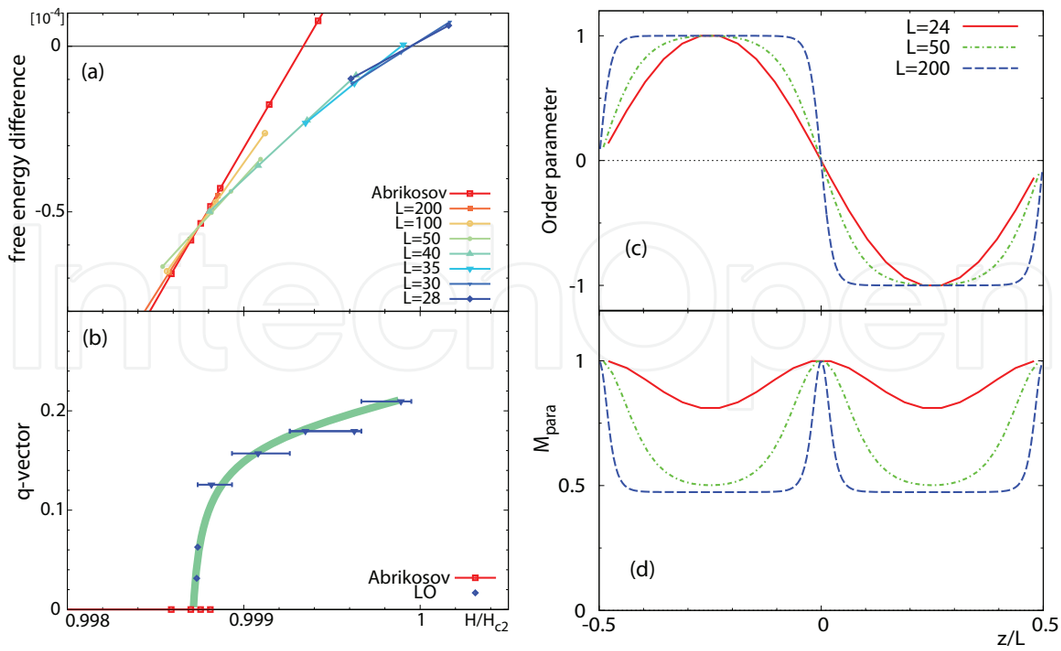

Fig. 13. (a) Field dependence of free energy F for conventional Abrikosov vortex state ($q = 0$) and FFLO vortex state for some $q = 2\pi/L(\neq 0)$. (b) Field dependence of FFLO wave number q estimated from (a). (c) Profile of pair potential $\Delta(\mathbf{r})$ along z-direction at midpoints between vortices for L =24, 50, 200. Normalized value $\Delta(\mathbf{r})/\Delta(z = -0.25L)$ is presented. (d) The same as (c) but for $M_{\text{para}}(\mathbf{r})$. We present normalized value $M_{\text{para}}(\mathbf{r})/M_{\text{para}}(z = 0)$. $\mu = 2$ and $T = 0.2T_c$.

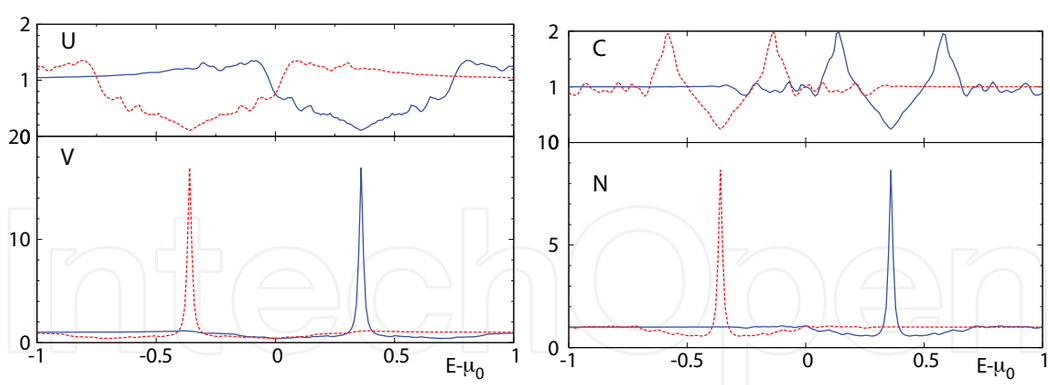

Fig. 14. Spectrum of the LDOS for up-spin electrons $N_\uparrow(E, \mathbf{r})/(0.5N_0)$ (solid lines) and for down-spin electrons $N_\downarrow(E, \mathbf{r})/(0.5N_0)$ (dashed lines) at positions U, V, N, and C, whose locations are shown in Fig. 2(a). $T = 0.2T_c$, $\bar{B} = 0.17985B_0$, and $L = 100R_0$ in the s-wave pairing.

Far from the FFLO nodal plane and outside of vortex, as shown in the spectrum at position U in Fig. 14, we see Zeeman shift of full-gap structure in s-wave superconductors. There, small LDOS also appears at low energies inside the gap due to the low energy excitations extending from the vortex cores and the FFLO nodal planes at finite magnetic fields. Since the LDOS are occupied at $E < 0$, and empty at $E > 0$, there is a relation of Eq. (18) between the

LDOS spectrum and local paramagnetic moment. Because of superconducting gap structure, the LDOS within superconducting gap is suppressed. Thus, difference of occupation number between up- and down-spin electrons is small, since the LDOS at $E < 0$ are occupied similarly in $N_\uparrow(E, \mathbf{r})$ and $N_\downarrow(E, \mathbf{r})$, except for small LDOS within the gap. This is the reason why $M_{\rm para}(\mathbf{r})$ is suppressed at the position U. Small but finite $M_{\rm para}(\mathbf{r})$ comes from the small LDOS weight of low energy states inside the gap at U in FFLO vortex states.

In the LDOS spectra at the position V on the vortex center and at the position N on the FFLO nodal plane presented in Fig. 14, $N_\uparrow(E, \mathbf{r})$ and $N_\downarrow(E, \mathbf{r})$, respectively, have a sharp peak at $E = \mu_+$ and $E = \mu_-$, with $\mu_\pm \equiv \mu_0 \pm \mu H$. These peaks are related to the topological structure of the pair potential, as schematically shown in Fig. 2. Since a vortex has phase winding 2π, along the trajectory through the vortex center, $\Delta(\mathbf{r})$ changes the sign by the π-phase shift across the vortex center. Also at the trajectory through the FFLO nodal plane, $\Delta(\mathbf{r})$ changes the sign across the nodal plane. The bound states appear as *zero-energy peak*, when the pair potential has the π-phase shift. This peak is shifted to $E = \mu_+$ or $E = \mu_-$ due to the Zeeman effect. Since the peak of the LDOS spectrum for up-spin electrons is an empty state ($E > 0$) and the peak of the LDOS for down-spin electrons is an occupied state ($E < 0$), $M_{\rm para}(\mathbf{r})$ becomes large at these positions, from the relation in Eq. (18).

On the other hand, along the trajectory through the intersection point of a vortex and a nodal plane, $\Delta(\mathbf{r})$ does not change the sign, because the phase shift is 2π by summing π due to vortex and π due to the nodal plane, as schematically shown in Fig. 2. Thus, the sharp peaks do not appear at $E = \mu_\pm$ as seen from the LDOS spectrum at the position C in Fig. 14. Instead, $N_\uparrow(E, \mathbf{r})$ has two broad peaks at finite energies shifted upper or lower from μ_+. In this situation, $M_{\rm para}(\mathbf{r})$ is still large at position C, as in positions V and N, since the LDOS in both peaks are empty ($E > 0$) in $N_\uparrow(E, \mathbf{r})$, and occupied ($E < 0$) in $N_\downarrow(E, \mathbf{r})$.

4.3 NMR spectrum in FFLO vortex states

In the NMR experiment, resonance frequency spectrum of the nuclear spin resonance is determined by the internal magnetic field and the hyperfine coupling to the spin of the conduction electrons. Therefore, in a simple consideration, the effective field for the nuclear spin is given by $B_{\rm eff}(\mathbf{r}) = B_z(\mathbf{r}) + A_{\rm hf} M_{\rm para}(\mathbf{r})$, where $A_{\rm hf}$ is a hyperfine coupling constant depending on species of the nuclear spins. The resonance line shape of NMR is given by

$$P(\omega) = \int \delta(\omega - B_{\rm eff}(\mathbf{r}))\mathrm{d}\mathbf{r}, \tag{20}$$

i.e., the intensity at each resonance frequency ω comes from the volume satisfying $\omega = B_{\rm eff}(\mathbf{r})$ in a unit cell. When the contribution of the hyperfine coupling is dominant, the NMR signal selectively detects $M_{\rm para}(\mathbf{r})$. This is the experiment observing the Knight shift in superconductors. As the NMR spectrum of the Knight shift, we calculate the distribution function $P(M) = \int \delta(M - M_{\rm para}(\mathbf{r}))\mathrm{d}\mathbf{r}$ from the spatial structure of the paramagnetic moment $M_{\rm para}(\mathbf{r})$ shown in Fig. 12(b). On the other hand, in the case of negligible hyperfine coupling, the NMR signal is determined by the internal magnetic field distribution. This resonance line shape is called *Redfield pattern* of the vortex lattice. The distribution function $P(B) = \int \delta(B - B_z(\mathbf{r}))\mathrm{d}\mathbf{r}$ is calculated from the internal field $B_z(\mathbf{r})$.

First we discuss the line shape of the distribution function $P(M)$, shown in Fig. 15(a). The spectrum of $P(M)$ in the conventional vortex state without FFLO modulation is shown by the lowest line in Fig. 15(a). There, the peak of $P(M)$ comes from the signal from the outside of the vortex core. Shift of the peak position from M_0 gives Knight shift in superconductors. The

spectrum of $P(M)$ has a tail toward larger M by the vortex core contribution of large $M_{\text{para}}(\mathbf{r})$. The vortex core contribution is a one-dimensional (1D) structure, their volume contribution is small in the spectrum, compared with the peak intensity due to the large volume contribution from outside of the vortex core. After the FFLO transition, the line shape $P(M)$ becomes double peak structure in the FFLO vortex states, as presented by upper lines in Fig. 15(a). The height of the main peak decreases, and there appears a new peak coming from the FFLO nodal plane near $M_{\text{para}} \sim M_0$. The contribution from 2D structure of the FFLO nodal plane appears in $P(M)$ more clearly than that of the 1D structure of the vortex line. When the period L becomes shorter at higher H, new peak at M_0 is enhanced, because the relative volume ratio of region near FFLO nodal plane becomes larger.

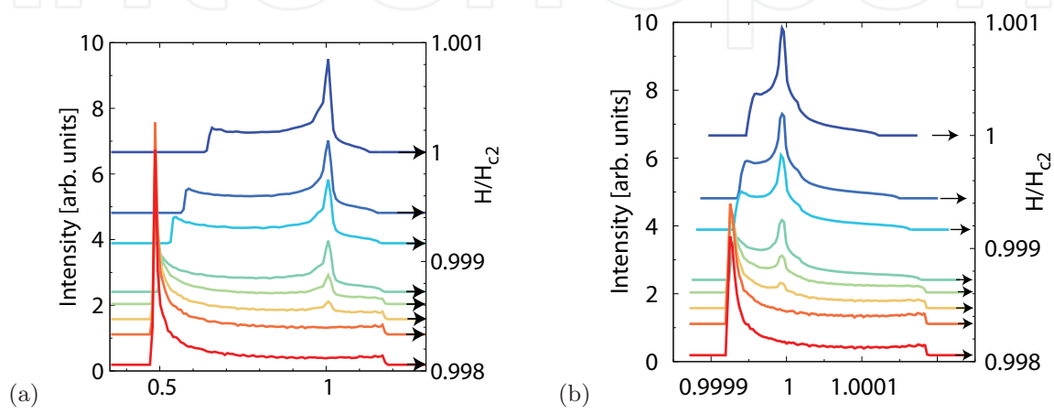

Fig. 15. (a) Distribution function of the paramagnetic moment. We show $P(M)$ as a function of M_{para}/M_0. (b) Distribution function of the internal magnetic field. We show $P(B)$ as a function of $B_z/\overline{B}$. $T = 0.2T_c$ and $\mu = 2$. Right-side axis pointed by arrows from each line indicates applied field H/H_{c2} for each NMR spectrum. Lowest line is for conventional Abrikosov vortex state of $q = 0$. Other upper lines are for FFLO vortex states. The heights of $P(M)$ and $P(B)$ are scaled so that $\int P(M)\mathrm{d}M = \int P(B)\mathrm{d}B = 1$.

Second, we discuss the distribution function $P(B)$ of the internal magnetic field, presented in Fig. 15(b). There, in the absence of the FFLO modulation (the lowest line), the Redfield pattern $P(B)$ has sharp peak corresponding to saddle points of the internal field distribution. The tail to higher B comes from the vortex core region of larger $B_z(\mathbf{r})$. In the presence of the FFLO modulation (other upper lines), the height of the original peak is decreased, and a new peak appears at $B \sim \bar{B}$ as the contribution of the FFLO nodal plane. In the line shape of $P(B)$, new peak by FFLO nodal plane is located near original saddle-point peak, compared with the line shape of $P(M)$. When the period L becomes shorter at higher H, new peak at $\overline{B}$ is enhanced. The experimental observation of the NMR resonance line shape is a method to identify the FFLO vortex state in high-field phase of $CeCoIn_5$ (Kakuyanagi et al., 2005; Kumagai et al., 2006; 2011). For $H \parallel c$, the NMR spectrum shows the double peak structure in the FFLO phase, appearing new peak in addition to the main peak in the vortex state. For $H \parallel ab$, we see double peak structure in NMR spectrum, but it reflects magnetic moments of SDW state (Koutroulakis et al., 2010; Young et al., 2007). The SDW structure in high field phase was observed also by neutron scattering (Kenzelmann et al., 2010; 2008). However, in NMR experiments at some species of nuclear spin, we can observe $P(M)$ or $P(B)$, excluding the signal by SDW (Kumagai et al., 2011). Thus, we expect that the relation of the SDW and FFLO for $H \parallel ab$ will be clarified in future studies.

4.4 Small Angle Neutron Scattering (SANS) in FFLO vortex states

The modulation of the internal magnetic field $B_z(\mathbf{r})$ may be observed by SANS experiment. If the periodic modulation along the z-direction is observed, it can be direct evidence of the FFLO modulation. Therefore, we discuss the neutron scattering in the FFLO vortex state. The intensity of the (h,k,l)-diffraction peak is given by $I_{h,k,l} = |F_{h,k,l}|^2/|q_{h,k,l}|$ with the wave vector $\mathbf{q}_{h,k,l}$ given in Eq. (12). Here we write $(m_1, m_2, m_3) = (h,k,l)$ following notations of the neutron scattering. The Fourier component $F_{h,k,l}$ is given by $B_z(\mathbf{r}) = \sum_{h,k,l} F_{h,k,l} \exp(\mathrm{i}\mathbf{q}_{h,k,l} \cdot \mathbf{r})$. The spots at $(h,k,l) = (1,0,0)$ and $(0,1,0)$ are used to determine the configuration and the orientation of the vortex lattice in SANS experiments (Bianchi et al., 2008; DeBeer-Schmitt et al., 2006), and the higher component $F_{h,k,0}$ is used to estimate the detailed structure of the internal magnetic field $B_z(\mathbf{r})$ (Kealey et al., 2000; White et al., 2010). It is noted that $F_{0,0,0} = \bar{B}$ and $F_{0,0,l} = 0$ for $l \neq 0$, because average flux density $\bar{B}$ within the unit cell of the vortex lattice is constant along the z-direction. Therefore, to detect the FFLO modulation, we have to use the spot $(1,0,2)$. The spot $(1,0,2)$ is near the spot $(1,0,0)$, which is used in the conventional SANS experiment to observe the stable vortex lattice configuration.

Change of intensity $|F_{1,0,0}|^2$ in the FFLO vortex state is presented in Fig. 16(a). This shows narrow H-range near H_{c2} among the H-dependence of $|F_{1,0}|^2$ in Fig. 8. After the transition from conventional Abrikosov vortex state (q=0) to FFLO vortex state ($q \neq 0$), $|F_{1,0,0}|^2$ shows rapid decrease. This is because $B_z(\mathbf{r})$ of vortex core expands at FFLO nodal plane, and the contrast of $B_z(\mathbf{r})$ between vortex core and outside is smeared after the average along the z-direction. When L becomes shorter at higher H, the relative volume ratio of the FFLO nodal plane increases, and $|F_{1,0,0}|^2$ decreases. As presented in Fig. 16(b), intensity $|F_{1,0,2}|^2$ for the signal of the FFLO vortex state appears at the FFLO transition. When L becomes shorter at higher H, $|F_{1,0,2}|^2$ decreases, due to the overlap between neighbor FFLO nodal regions.

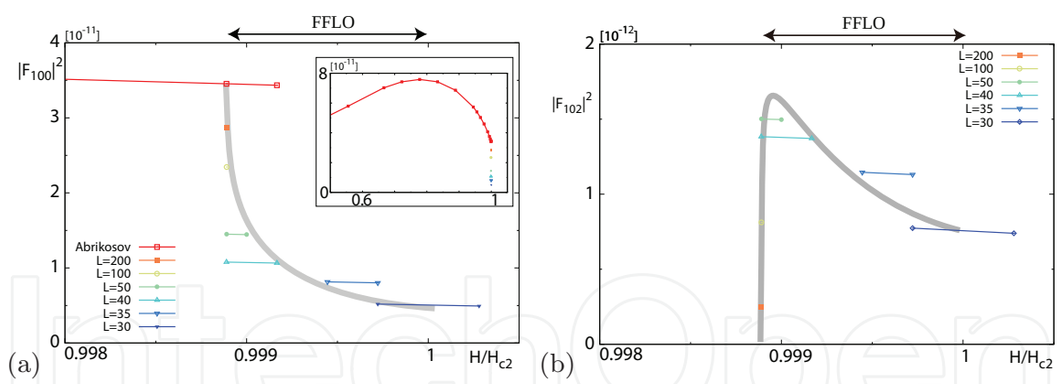

Fig. 16. Magnetic field dependence of FLL form factor $|F_{1,0,0}|^2$ (a) and $|F_{1,0,2}|^2$ (b) in FFLO vortex states. FFLO wave number $q = 2\pi/L$ at each H is given in Fig. 13. $T = 0.2T_c$ and $\mu = 2$. Lines are guide for the eye. Inset in (a) presents wider H-range.

5. Summary and discussion

We discussed interesting phenomena of vortex states in superconductors with strong paramagnetic effect, based on quasi-classical Eilenberger theory. The paramagnetic effect comes from splitting of up-spin and down-spin Fermi surfaces due to the Zeeman effect. In our calculations, since spatial structures of the order parameter and the internal field are calculated in vortex lattice states self-consistently with local electronic states, we

can quantitatively estimate the field dependence of physical quantities from obtained quasi-classical Green's functions in Eilenberger theory. These theoretical calculations give helpful information to evaluate contributions of pairing symmetries and paramagnetic effects etc. in experimental data observing physical properties of vortex states in unconventional superconductors.

First, we discussed anomalous field dependence of physical quantities by strong paramagnetic effect in vortex states at lower fields than the FFLO transition. Calculating the spatial structure of the vortex states and local electronic states, we clarified the paramagnetic effects in the vortex core structure. There, the core radius is enlarged and the internal field around the core is further enhanced, due to the enhanced paramagnetic moments at the vortex core. This occurs as a result of Zeeman splitting of bound electronic states at the vortex core. We estimated the magnetic field dependence of low temperature specific heat, Knight shift, magnetization, and flux line lattice form factor. There we found anomalous field dependence when the paramagnetic effect is strong. The specific heat, Knight shift, and magnetization show rapid increase near H_{c2}, due to the paramagnetic pair breaking which is eminent at higher fields. Anomalous enhancement of the FLL form factor as a function of magnetic field observed in $CeCoIn_5$ may reflect the paramagnetic vortex core structure by the strong paramagnetic effect. We quantitatively compared the anomalous magnetic field dependence of specific heat, magnetization curve, and the FLL form factor observed in $CeCoIn_5$ with results of our theoretical calculations. The paramagnetic effect can explain the anomalous field dependences qualitatively. However we found systematic quantitative deviation between the theory and the experimental data. Therefore, we showed that the deviation can be improved by considering phenomenological field dependence of normal state density of states, which reflects mass enhancement near quantum critical point at H_{c2}.

Next, we studied the FFLO states coexisting with vortices. When the paramagnetic effect is very strong, at high magnetic fields we can expect a transition to the FFLO phase where the order parameter has periodic oscillation originating from the Zeeman splitting of the Fermi surface. To discuss the FFLO states suggested in high field phase of $CeCoIn_5$, we have to consider vortices in addition to the FFLO modulation. By Eilenberger theory, we selfconsistently calculated fully 3D spatial structure of the pair potential, the internal magnetic field, the paramagnetic moment, and local electronic states in the vortex lattice state with FFLO nodal planes perpendicular to vortex lines. In the FFLO vortex states, topological structures of the pair potential determine their qualitative properties. At the FFLO nodal plane or at the vortex line, π-phase shift of the pair potential gives rise to sharp peaks in the LDOS at Fermi level of electronic states, and the Zeeman shift of the peaks enhances the local paramagnetic moment. Based on these spatial structures, we discussed NMR spectrum and neutron scattering, to identify characteristic behaviours in the FFLO states. We estimated the period of FFLO modulation and the phase diagram as a function of magnetic field H, and discussed the field dependence of NMR spectrum and FLL form factors in the FFLO vortex states. We hope that these features will be used to identify the FFLO vortex structure in the high-field phase of $CeCoIn_5$ for $H \parallel c$ and for $H \parallel ab$. For the latter, the FLLO modulation may coexist with SDW states.

6. Acknowledgments

The authors are grateful for useful discussions and communications with T. Mizushima, H. Adachi, N. Nakai, K. Kumagai, Y. Matsuda, and M.R. Eskildsen.

7. References

Adachi, H., Ichioka, M. & Machida, K. (2005). Mixed-state thermodynamics of a superconductor with moderately large paramagnetic effects, *J. Phys. Soc. Jpn.* 74: 2181–2184.

Adachi, H. & Ikeda, R. (2003). Effects of Pauli paramagnetism on the superconducting vortex phase diagram in strong fields, *Phys. Rev. B* 68: 184510, 1–17.

Bianchi, A. D., Kenzelmann, M., DeBeer-Schmitt, L., White, J. S., Forgan, E. M., Mesot, J., Zolliker, M., Kohlbrecher, J., Movshovich, R., Bauer, E. D., Sarrao, J. L., Fisk, Z., Petrović, C. & Eskildsen, M. R. (2008). Superconducting vortices in $CeCoIn_5$: Toward the Pauli-limiting field, *Science* 319: 177–180.

Bianchi, A., Movshovich, R., Capan, C., Pagliuso, P. G. & Sarrao, J. (2003). Possible Fulde-Ferrell-Larkin-Ovchinnikov superconducting state in $CeCoIn_5$, *Phys. Rev. Lett.* 91: 187004, 1–4.

Bianchi, A., Movshovich, R., Oeschler, N., Gegenwart, P., Steglich, F., Thompson, J. D., Pagliuso, P. G. & Sarrao, J. (2002). First-order superconducting phase transition in $CeCoIn_5$, *Phys. Rev. Lett.* 89: 137002, 1–4.

Bianchi, A., Movshovich, R., Vekhter, I., Pagliuso, P. & Sarrao, J. (2003). Field dependent coherence length in the superclean, high-κ superconductor $CeCoIn_5$, *Phys. Rev. Lett.* 91: 257001, 1–4.

Casalbuoni, R. & Nardulli, G. (2004). Inhomogeneous superconductivity in condensed matter and QCD, *Rev. Mod. Phys.* 76: 263–320.

DeBeer-Schmitt, L., Dewhurst, C. D., Hoogenboom, B. W., Petrović, C. & Eskildsen, M. R. (2006). Field dependent coherence length in the superclean, high-κ superconductor $CeCoIn_5$, *Phys. Rev. Lett.* 97: 127001, 1–4.

DeBeer-Schmitt, L., Eskildsen, M., Ichioka, M., Machida, K., Jenkins, N., Dewhurst, C. D., Abrahamsen, A. B., Bud'ko, S. L. & Canfield, P. (2007). Pauli paramagnetic effects on vortices in superconducting $TmNi_2B_2C$, *Phys. Rev. Lett.* 99: 167001, 1–4.

Doria, M. M., Gubernatis, J. E. & Rainer, D. (1990). Solving the Ginzburg-Landau equations by simulated annealing, *Phys. Rev. B* 41: 6335–6340.

Eilenberger, G. (1968). Transformation of Gorkov's equation for type II superconductors into transport-like equations, *Z. Phys.* 214: 195–213.

Fetter, A. L. & Hohenberg, P. C. (1969). Theory of type II superconductors, *in* R. D. Parks (ed.), *Superconductivity*, Dekker, New York, pp. 817–923(Chap.14).

Fulde, P. & Ferrell, R. (1964). Superconductivity in a strong spin-exchange field, *Phys. Rev.* 135: A550–A563.

Hayashi, N., Ichioka, M. & Machida, K. (1996). Star-shaped local density of states around vortices in a type-II superconductor, *Phys. Rev. Lett.* 77: 4074–4077.

Hayashi, N., Ichioka, M. & Machida, K. (1997). Effects of gap anisotropy upon the electronic structure around a superconducting vortex, *Phys. Rev. B* 56: 9052–9063.

Hess, H. F., Robinson, R. B. & Waszczak, J. V. (1990). Vortex-core structure observed with a scanning tunneling microscope, *Phys. Rev. Lett.* 64: 2711–2714.

Hiragi, M., Suzuki, K., Ichioka, M. & Machida, K. (2010). Vortex state and field-angle resolved specific heat oscillation for H//ab in d-wave superconductors, *J. Phys. Soc. Jpn.* 79: 094709, 1–9.

Houzet, M. & Buzdin, A. (2001). Structure of the vortex lattice in the Fulde-Ferrell-Larkin-Ovchinnikov state, *Phys. Rev. B* 63: 184521, 1–5.

Ichioka, M., Adachi, H., Mizushima, T. & Machida, K. (2007). Vortex state in a Fulde-Ferrell-Larkin-Ovchinnikov superconductor based on quasiclassical theory, *Phys. Rev. B* 76: 014503, 1–10.

Ichioka, M., Hasegawa, A. & Machida, K. (1999a). Field dependence of the vortex structure in d-wave and s-wave superconductors, *Phys. Rev. B* 59: 8902–8916.

Ichioka, M., Hasegawa, A. & Machida, K. (1999b). Vortex lattice effects on low-energy excitations in d-wave and s-wave superconductors, *Phys. Rev. B* 59: 184–187.

Ichioka, M., Hayashi, N., Enomoto, N. & Machida, K. (1996). Vortex structure in d-wave superconductors, *Phys. Rev. B* 53: 15316–15326.

Ichioka, M., Hayashi, N. & Machida, K. (1997). Local density of states in the vortex lattice in a type-II superconductor, *Phys. Rev. B* 55: 6565–6576.

Ichioka, M. & Machida, K. (2007). Vortex states in superconductors with strong Pauli-paramagnetic effect, *Phys. Rev. B* 76: 064502, 1–7.

Ikeda, R. & Adachi, H. (2004). Modulated vortex lattice in high fields and gap nodes, *Phys. Rev. B* 69: 212506, 1–4.

Ikeda, S., Shishido, H., Nakashima, M., Settai, R., Aoki, D., Haga, Y., Harima, H., Aoki, Y., Namiki, T., Sato, H. & Onuki, Y. (2001). Unconventional superconductivity in $CeCoIn_5$ studied by the specific heat and magnetization measurements, *J. Phys. Soc. Jpn.* 70: 2248–2251.

Izawa, K., Yamaguchi, H., Matsuda, Y., Shishido, H., Settai, R. & Onuki, Y. (2001). Angular position of nodes in the superconducting gap of quasi-2D heavy-fermion superconductor $CeCoIn_5$, *Phys. Rev. Lett.* 87: 057002, 1–4.

Kakuyanagi, K., Saitoh, M., Kumagai, K., Takashima, S., Nohara, M., Takagi, H. & Matsuda, Y. (2005). Texture in the superconducting order parameter of $CeCoIn_5$ revealed by nuclear magnetic resonance, *Phys. Rev. Lett.* 94: 047602, 1–4.

Kealey, P. G., Riseman, T. M., Forgan, E. M., Galvin, L. M., Mackenzie, A. P., Lee, S. L., Paul, D. M., Cubitt, R., Agterberg, D. F., Heeb, R., Mao, Z. Q. & Maeno, Y. (2000). Reconstruction from small-angle neutron scattering measurements of the real space magnetic field distribution in the mixed state of Sr_2RuO_4, *Phys. Rev. Lett.* 84: 6094–6097.

Kenzelmann, M., Gerber, S., Egetenmeyer, N., Gavilano, J. L., Strässle, T., Bianchi, A. D., Ressouche, E., Movshovich, R., Bauer, E. D., Sarrao, J. L. & Thompson, J. D. (2010). Evidence for a magnetically driven superconducting Q phase of $CeCoIn_5$, *Phys. Rev. Lett.* 104: 127001, 1–4.

Kenzelmann, M., Strässle, T., Niedermayer, C., Sigrist, M., Padmanabhan, B., Zolliker, M., Bianchi, A. D., Movshovich, R., Bauer, E. D., Sarrao, J. L. & Thompson, J. D. (2008). Coupled superconducting and magnetic order in $CeCoIn_5$, *Science* 321: 1652–1654.

Klein, U. (1987). Microscopic calculations on the vortex state of type II superconductors, *J. Low Temp. Phys.* 69: 1–37.

Klein, U., Rainer, D. & Shimahara, H. (2000). Interplay of Fulde-Ferrell-Larkin-Ovchinnikov and vortex states in two-dimensional superconductors, *J. Low Temp. Phys.* 118: 91–104.

Koutroulakis, G., Stewart, Jr. M. D., Mitrović, V. F., Horvatić, M., Berthier, C., Lapertot, G. & Flouquet, J. (2010). Field evolution of coexisting superconducting and magnetic orders in $CeCoIn_5$, *Phys. Rev. Lett.* 104: 087001, 1–4.

Kumagai, K., Saitoh, M., Oyaizu, T., Furukawa, Y., Takashima, S., Nohara, M., Takagi, H. & Matsuda, Y. (2006). Fulde-Ferrell-Larkin-Ovchinnikov state in a perpendicular field of quasi-two-dimensional $CeCoIn_5$, *Phys. Rev. Lett.* 97: 227002, 1–4.

Kumagai, K., Shishido, H., Shibauchi, T. & Matsuda, Y. (2011). Evolution of paramagnetic quasiparticle excitations emerged in the high-field superconducting phase of $CeCoIn_5$. Preprint, arXiv:1103.1440 (to appear in *Phys. Rev. Lett.*).

Larkin, A. I. & Ovchinnikov, Y. N. (1965). Inhomogeneous state of superconductors, *Sov. Phys. JETP* 20: 762–769.

Machida, K., Mizushima, T. & Ichioka, M. (2006). Generic phase diagram of fermion superfluids with population imbalance, *Phys. Rev. Lett.* 97: 120407, 1–4.

Machida, K. & Nakanishi, H. (1984). Superconductivity under a ferromagnetic molecular field, *Phys. Rev. B* 30: 122–133.

Matsuda, Y. & Shimahara, H. (2007). Fulde-Ferrell-Larkin-Ovchinnikov state in heavy fermion superconductors, *J. Phys. Soc. Jpn.* 76: 051005, 1–16.

Miranović, P. & Machida, K. (2003). Thermodynamics and magnetic field profiles in low-κ type-II superconductors, *Phys. Rev. B* 67: 092506, 1–4.

Miranović, P., Nakai, N., Ichioka, M. & Machida, K. (2003). Orientational field dependence of low-lying excitations in the mixed state of unconventional superconductors, *Phys. Rev. B* 68: 052501, 1–4.

Mizushima, T., Machida, K. & Ichioka, M. (2005a). Direct imaging of spatially modulated superfluid phases in atomic fermion systems, *Phys. Rev. Lett.* 94: 060404, 1–4.

Mizushima, T., Machida, K. & Ichioka, M. (2005b). Topological structure of a vortex in the Fulde-Ferrell-Larkin-Ovchinnikov state, *Phys. Rev. Lett.* 95: 117003, 1–4.

Moler, K. A., Baar, D. J., Urbach, J. S., Liang, R., Hardy, W. N. & Kapitulnik, A. (1994). Magnetic field dependence of the density of states of $YBa_2Cu_3O_{6.95}$ as determined from the specific heat, *Phys. Rev. B* 73: 2744–2747.

Nakai, N., Miranović, P., Ichioka, M. & Machida, K. (2004). Field dependence of the zero-energy density of states around vortices in an anisotropic-gap superconductor, *Phys. Rev. B* 70: 100503(R), 1–4.

Nishimori, H., Uchiyama, K., Kaneko, S., Tokura, A., Takeya, H., Hirata, K. & Nishida, N. (2004). First observation of the fourfold-symmetric and quantum regime vortex core in YNi_2B_2C by scanning tunneling microscopy and spectroscopy, *J. Phys. Soc. Jpn.* 73: 3247–3250.

Nohara, M., Isshiki, M., Sakai, F. & Takagi, H. (1999). Quasiparticle density of states of clean and dirty s-wave superconductors in the vortex state, *J. Phys. Soc. Jpn.* 68: 1078–1081.

Paglione, J., Tanatar, M. A., Hawthorn, D. G., Boaknin, E., Hill, R. W., Ronning, F., Sutherland, M., Taillefer, L., Petrovic, C. & Canfield, P. (2003). Field-induced quantum critical point in $CeCoIn_5$, *Phys.Rev. Lett.* 91: 246405, 1–4.

Partridge, G. B., Li, W., Kamar, R. I., Liao, Y. & Hulet, R. (2006). Pairing and phase separation in a polarized fermi gas, *Science* 311: 503–505.

Radovan, H. A., Fortune, N. A., Murphy, T. P., Hannahs, S. T., Palm, E. C., Tozer, S. W. & Hall, D. (2003). Magnetic enhancement of superconductivity from electron spin domains, *Nature (London)* 425: 51–55.

Ramirez, A. P., Varma, C. M., Fisk, Z. & Smith, J. L. (1999). Fermi-liquid renormalization in the superconducting state of UBe_{13}, *Philos. Mag. B* 79: 111–117.

Schopohl, N. & Maki, K. (1995). Quasiparticle spectrum around a vortex line in a d-wave superconductor, *Phys. Rev. B* 52: 490–493.

Shimahara, H. (1994). Fulde-Ferrell state in quasi-two-dimensional superconductors, *Phys. Rev. B* 50: 12760–12765.

Tachiki, M., Takahashi, S., Gegenwart, P., Weiden, M., Lang, M., Geibel, C., Steglich, F., Modler, R., Paulsen, C. & Onuki, Y. (1996). Generalized Fulde-Ferrell-Larkin-Ovchinnikov state in heavy-fermion and intermediate-valence systems, *Z. Physik B* 100: 369–380.

Takahashi, M., Mizushima, T., Ichioka, M. & Machida, K. (2006). Vortex-core structure in neutral fermion superfluids with population imbalance, *Phys. Rev. Lett.* 97: 180407, 1–4.

Tayama, T., Harita, A., Sakakibara, T., Haga, Y., Shishido, H., Settai, R. & Onuki, Y. (2002). Unconventional heavy-fermion superconductor $CeCoIn_5$: dc magnetization study at temperatures down to 50 mK, *Phys. Rev. B* 65: 180504(R), 1–4.

Volovik, G. E. (1993). Superconductivity with lines of gap nodes: density of states in the vortex, *JETP Lett.* 58: 469–473.

Watanabe, K., Kita, T. & Arai, M. (2005). Magnetic-field dependence of thermodynamic quantities in the vortex state of type-II superconductors, *Phys. Rev. B* 71: 144515, 1–8.

White, J. S., Das, P., Eskildsen, M. R., DeBeer-Schmitt, L., Forgan, E. M., Bianchi, A. D., Kenzelmann, M., Zolliker, M., Gerber, S., Gavilano, J. L., Mesot, J., Movshovich, R., Bauer, E. D., Sarrao, J. L. & Petrović, C. (2010). Observations of Pauli paramagnetic effects on the flux line lattice in $CeCoIn_5$, *New J. Phys.* 12: 023026, 1–11.

Yano, K., Sakakibara, T., Tayama, T., Yokoyama, M., Amitsuka, H., Homma, Y., Miranović, P., Ichioka, M., Tsutsumi, Y. & Machida, K. (2008). Field-angle-dependent specific heat measurements and gap determination of a heavy fermion superconductor URu_2Si_2, *Phys. Rev. Lett.* 100: 017004, 1–4.

Young, B.-L., Urbano, R., Curro, N., Thompson, J., Sarrao, J. L., Vorontsov, A. B. & Graf, M. (2007). Microscopic evidence for field-induced magnetism in $CeCoIn_5$, *Phys. Rev. Lett.* 98: 036402, 1–4.

Zheng, G. -q., Ozaki, H., Kitaoka, Y., Kuhns, P., Reyes, A. & Moulton, W. (2002). Delocalized quasiparticles in the vortex state of an overdoped high- T_c superconductor probed by ^{63}Cu NMR, *Phys. Rev. Lett.* 88: 077003, 1–4.

Zwierlein, M. W., Schirotzek, A., Schunck, C. H. & Ketterle, W. (2006). Fermionic superfluidity with imbalanced spin populations, *Science* 311: 492–496.

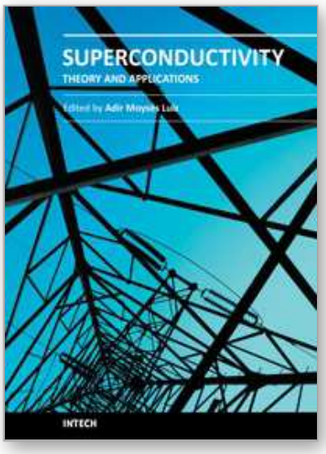

Superconductivity - Theory and Applications

Edited by Dr. Adir Luiz

ISBN 978-953-307-151-0
Hard cover, 346 pages
Publisher InTech
Published online 18, July, 2011
Published in print edition July, 2011

Superconductivity was discovered in 1911 by Kamerlingh Onnes. Since the discovery of an oxide superconductor with critical temperature (Tc) approximately equal to 35 K (by Bednorz and Müller 1986), there are a great number of laboratories all over the world involved in research of superconductors with high Tc values, the so-called â€œHigh-Tc superconductorsâ€. This book contains 15 chapters reporting about interesting research about theoretical and experimental aspects of superconductivity. You will find here a great number of works about theories and properties of High-Tc superconductors (materials with Tc > 30 K). In a few chapters there are also discussions concerning low-Tc superconductors (Tc < 30 K). This book will certainly encourage further experimental and theoretical research in new theories and new superconducting materials.

How to reference

In order to correctly reference this scholarly work, feel free to copy and paste the following:

Masanori Ichioka, Kenta M. Suzuki, Yasumasa Tsutsumi and Kazushige Machida (2011). FFLO and vortex states in superconductors with strong paramagnetic effect, Superconductivity - Theory and Applications, Dr. Adir Luiz (Ed.), ISBN: 978-953-307-151-0, InTech, Available from: http://www.intechopen.com/books/superconductivity-theory-and-applications/fflo-and-vortex-states-in-superconductors-with-strong-paramagnetic-effect

INTECH
open science | open minds

InTech Europe
University Campus STeP Ri
Slavka Krautzeka 83/A
51000 Rijeka, Croatia
Phone: +385 (51) 770 447
Fax: +385 (51) 686 166
www.intechopen.com

InTech China
Unit 405, Office Block, Hotel Equatorial Shanghai
No.65, Yan An Road (West), Shanghai, 200040, China
中国上海市延安西路65号上海国际贵都大饭店办公楼405单元
Phone: +86-21-62489820
Fax: +86-21-62489821